

Article

Discovery of Novel Spiro[3H-indole-3,2'-pyrrolidin]-2(1H)-one Compounds as Chemically Stable, and Orally Active Inhibitors of the MDM2-p53 Interaction

Andreas Gollner, Dorothea Rudolph, Heribert Arnhof, Markus Bauer, Sophia Maria Blake, Guido Boehmelt, Xiao-Ling Cockcroft, Georg Dahmann, Peter Ettmayer, Thomas Gerstberger, Jale Karolyi-Oezguer, Dirk Kessler, Christiane Kofink, Juergen Ramharter, Jörg Rinnenthal, Alexander Savchenko, Renate Schnitzer, Harald Weinstabl, Ulrike Weyer-Czernilofsky, Tobias Wunberg, and Darryl B. McConnell

J. Med. Chem., **Just Accepted Manuscript** • DOI: 10.1021/acs.jmedchem.6b00900 • Publication Date (Web): 24 Oct 2016

Downloaded from <http://pubs.acs.org> on October 24, 2016

Just Accepted

"Just Accepted" manuscripts have been peer-reviewed and accepted for publication. They are posted online prior to technical editing, formatting for publication and author proofing. The American Chemical Society provides "Just Accepted" as a free service to the research community to expedite the dissemination of scientific material as soon as possible after acceptance. "Just Accepted" manuscripts appear in full in PDF format accompanied by an HTML abstract. "Just Accepted" manuscripts have been fully peer reviewed, but should not be considered the official version of record. They are accessible to all readers and citable by the Digital Object Identifier (DOI®). "Just Accepted" is an optional service offered to authors. Therefore, the "Just Accepted" Web site may not include all articles that will be published in the journal. After a manuscript is technically edited and formatted, it will be removed from the "Just Accepted" Web site and published as an ASAP article. Note that technical editing may introduce minor changes to the manuscript text and/or graphics which could affect content, and all legal disclaimers and ethical guidelines that apply to the journal pertain. ACS cannot be held responsible for errors or consequences arising from the use of information contained in these "Just Accepted" manuscripts.



ACS Publications

Journal of Medicinal Chemistry is published by the American Chemical Society, 1155 Sixteenth Street N.W., Washington, DC 20036

Published by American Chemical Society. Copyright © American Chemical Society. However, no copyright claim is made to original U.S. Government works, or works produced by employees of any Commonwealth realm Crown government in the course of their duties.

Discovery of Novel Spiro[3H-indole-3,2'-pyrrolidin]-2(1H)-one Compounds as Chemically Stable, and Orally Active Inhibitors of the MDM2–p53 Interaction

Andreas Gollner,^{*,†} Dorothea Rudolph[†], Heribert Arnhof[†], Markus Bauer[†], Sophia M. Blake[†], Guido Boehmelt[†], Xiao-Ling Cockcroft[†], Georg Dahmann[‡], Peter Ettmayer[†], Thomas Gerstberger[†], Jale Karolyi-Oezguer[†], Dirk Kessler[†], Christiane Kofink[†], Juergen Ramharter[†], Jörg Rinnenthal[†], Alexander Savchenko[†], Renate Schnitzer[†], Harald Weinstabl[†], Ulrike Weyer-Czernilofsky[†], Tobias Wunberg[†], and Darryl B. McConnell[†]

[†] Boehringer Ingelheim RCV GmbH & Co KG, Vienna, Austria

[‡] Boehringer Ingelheim Pharma GmbH & Co KG, Biberach, Germany

ABSTRACT

Scaffold modification based on Wang's pioneering MDM2-p53 inhibitors led to novel, chemically stable spiro-oxindole compounds bearing a spiro[3H-indole-3,2'-pyrrolidin]-2(1H)-one scaffold that are not prone to epimerization as observed for the initial spiro[3H-indole-3,3'-pyrrolidin]-2(1H)-one scaffold. Further structure based optimization inspired by natural product architectures led to a complex fused ring system ideally suited to bind to the MDM2 protein and to interrupt its protein-protein interaction (PPI) with TP53. The compounds are highly selective and show in vivo efficacy in a SJSA-1 xenograft model even when given as a single dose as demonstrated for 4-[(3S,3'S,3'aS,5'R,6'aS)-6-chloro-3'-(3-chloro-2-fluorophenyl)-1'-(cyclopropylmethyl)-2-oxo-1,2,3',3'a,4',5',6',6'a-octahydro-1'H-spiro[indole-3,2'-pyrrolo[3,2-b]pyrrole]-5'-yl]benzoic acid (BI-0252).

INTRODUCTION

The tumor protein p53 (TP53), the so called “guardian of the genome”, is a pivotal tumor suppressor protein and a mainstay of the body’s cellular anti-cancer defense system.¹ As a potent transcription factor, TP53 is activated following cellular stress and regulates multiple downstream target genes implicated in cell-cycle control, apoptosis, senescence and DNA repair.² *TP53* is one of the most frequently mutated genes in cancer with about 50% of all human cancers having mutations or deletions in this gene, although the incidence of *TP53* mutations differs significantly between different cancer types.^{3,4} Mice lacking TP53 develop normally but are prone to the spontaneous development of multiple types of cancer, particularly lymphomas and sarcomas, at an early age.⁵ Although the remaining 50% of human cancers have tumors with *TP53* wild-type status, the function of TP53 is frequently attenuated in these cancers by other mechanisms including overexpression of its key negative regulator HDM2, the human homolog of mouse double minute 2 (MDM2). Mice deficient for *MDM2* die early in embryonic development. Absence of TP53 rescues the embryonic lethality seen in MDM2-deficient mice, suggesting a critical role of MDM2 in the regulation of TP53 function.⁶ MDM2, an E3 ligase, regulates TP53 function and protein stability by three main mechanisms. First, MDM2 binds to the transactivation domain of TP53 and represses transcriptional activity of TP53. Secondly, MDM2 transports the transcription factor TP53 from the nucleus to the cytoplasm and third, the E3 ligase function of MDM2 facilitates proteasome-mediated TP53 protein degradation.⁷ Recent preclinical data show that genetic changes in *TP53* not only contribute to tumor development but also to continued tumor growth as restoration of TP53 function in established tumors by genetic means causes tumor regressions in preclinical models of cancer.⁸⁻¹⁰ Based on these data, stabilization and activation of wild-type TP53 by the inhibition of TP53 binding to its negative regulator MDM2 has recently been explored as a novel approach to cancer therapy.

Several MDM2-p53 PPI inhibitors are currently being evaluated in early clinical development¹¹ with daily dosing regimens, and recent clinical data suggest thrombocytopenia as an on-target, dose-limiting toxicity for this class of inhibitors.¹²⁻¹⁵ Thrombocytopenia could limit the clinical utility of MDM2-p53 inhibitors, hence there is a need for a less frequently dosed MDM2 inhibitor to allow clinical management of side effects. Therefore, we started investigations to identify a highly potent MDM2 inhibitor capable of achieving efficacy with less frequent dosing in mice.

Intense research over the past years has yielded several MDM2-p53 PPI inhibitors both from academia and industry.¹⁶⁻²⁰ It is interesting to note that many such inhibitors contain structural architectures akin to natural products displaying dense, spherical shapes with a high number of stereo centers rather than compounds prepared in a medicinal chemistry laboratory²¹⁻²⁴. Notably many scaffolds have been generated by multicomponent reactions in the course of initial hit-finding initiatives.²⁵⁻⁴¹ Herein we report the discovery of a new class of spiro-oxindoles as MDM2-p53 PPI inhibitors inspired by Wang's spiro[3*H*-indole-3,3'-pyrrolidin]-2(1*H*)-one inhibitors^{31, 42} and natural products^{43, 44} for which the potency and pharmacokinetic properties could be optimized to show in vivo efficacy when given as a single dose in a two week mouse SJSA-1 xenograft study.

Spiro-oxindoles as MDM2 Inhibitors. Spiro-oxindoles are promising scaffolds for anticancer agents⁴⁵ and have been identified as inhibitors of the MDM2-p53 interaction by Wang et al.^{31, 46} employing a structure-based de novo design. The indole ring of Trp23_(p53), which fills a hydrophobic cleft in the binding site (Trp23 pocket) and forms a key hydrogen bond with the backbone carbonyl of Leu54_(MDM2), was replaced by an oxindole. Inspired by complex natural product architectures like Spirotryprostatin B (Scheme 1) the Wang group utilized additional valency at the C3 (Scheme 2) of the oxindole to install a spiro-ring and consequentially spiro[3*H*-indole-3,3'-pyrrolidin]-2(1*H*)-ones were designed. This scaffold

offered excellent vectors to address the remaining two lipophilic MDM2 cavities (Leu26_(p53)- and Phe19_(p53)-pockets) of the TP53 binding site and led to several MDM2-p53 inhibitors¹⁶ such as the Sanofi-Aventis clinical spiroindolinone derivative (2'S,3R,4'S,5'R)-6-chloro-4'-(3-chloro-2-fluorophenyl)-2'-(2,2-dimethylpropyl)-N-(4-hydroxycyclohexyl)-2-oxo-1,2-dihydrospiro[indole-3,3'-pyrrolidine]-5'-carboxamide (SAR405838)⁴⁷ (Scheme 2, A). Additional spiro[3*H*-indole-3,3'-pyrrolidin]-2(1*H*)-one MDM2-p53 inhibitors have been reported by academia and industry including aza-oxindole derivative (2S,3R,4S,5R)-N-(4-carbamoylphenyl)-6'-chloro-4-(3-chloro-2-fluorophenyl)-2-(2,2-dimethylpropyl)-2'-oxo-1',2'-dihydrospiro[pyrrolidine-3,3'-pyrrolo[3,2-*c*]pyridine]-5-carboxamide (RO2468)⁴⁸ (Scheme 2, A) along with other potent preclinical compounds from Hoffmann-La Roche^{48, 49} and the recently disclosed clinical spiro-oxindole derivative (3'R,4'S,5'R)-N-[(6S)-6-carbamoyloxan-3-yl]-6'-chloro-4'-(2-chloro-3-fluoropyridin-4-yl)-4,4-dimethyl-2"-oxo-1",2"-dihydrodispiro[cyclohexane-1,2'-pyrrolidine-3',3"-indole]-5'-carboxamide (DS-3032b)⁵⁰ with symmetrical pyrrolidine C2 substitution by Daiichi Sankyo (Scheme 2, A). Additional spiro-oxindoles lead compounds have been identified by hit-finding initiatives^{25, 51}, by the synthesis of bioisosters of spiro[3*H*-indole-3,3'-pyrrolidin]-2(1*H*)-ones like spiro(oxindole-thiazolidine)-based derivatives^{52, 53} or recently published spiro[3*H*-indole-3,2'-pyrrolidin]-2(1*H*)-one compounds that interestingly show a very different binding mode compared to the initial compounds^{34, 54}, and others^{33, 35, 36, 55}.

Spiro[3*H*-indole-3,3'-pyrrolidin]-2(1*H*)-ones with a chiral center at C2 are associated with chemical instability since they can undergo equilibration to four diastereomers at C2 and C3 in solution by a reversible ring-opening retro-Mannich reaction under various conditions (Scheme 2, B) which was first recognized and shown by a X-ray co-crystal structure by Popowicz et al (3LBL)⁵⁶. The Wang group recently approached this liability by installing symmetrical pyrrolidine substituents which undergo rapid conversion to one stable diastereomer.^{42, 57} Our goal was to solve this issue by identifying a novel and stable spiro-

oxindole scaffold that is suited for further optimization to finally combine potency, chemical stability and good PK properties (Scheme 1).

RESULTS

Design of the New Scaffold. Based on the binding mode of known spiro-oxindole MDM2-p53 inhibitors we hypothesized that spiro[3*H*-indole-3,2'-pyrrolidin]-2(1*H*)-ones might bind similarly but would be chemically stable since the ring-opening retro-Mannich reaction cannot occur. In addition the new scaffold potentially offers vectors better suited to address additional interactions to improve binding affinity. We therefore prepared spiro-oxindole compounds **5a** and **5b** which were assumed to occupy the Trp23 pocket with their 6-chloro-oxindole (ring "A") and the Leu26 pocket with a 3-chloro-phenyl (ring "B"). The racemic mixture with the aromatic rings "A" and "B" in "trans" configuration indeed showed the expected biochemical activities with IC₅₀s (MDM2-p53) of 37 μM for **5a** and 40 μM for **5b** which were very comparable to the IC₅₀ (MDM2-p53) of 36 μM measured for the racemic spiro[3*H*-indole-3,3'-pyrrolidin]-2(1*H*)-one benchmark fragment **4** (Figure 1). The contribution of the nitro-group to the binding of **5a** and **5b**, which was solely incorporated for synthetic accessibility reasons through dipolar cycloaddition chemistry (see chemistry section) was not fully examined, however docking results suggested a polar interaction with His96 (Figure 2A). The reduction of **5b** to the primary amine gave racemic **1** which showed slightly weaker potency [IC₅₀ (MDM2-p53) = 74 μM]. The new spiro[3*H*-indole-3,2'-pyrrolidin]-2(1*H*)-one (**1**) was indeed stable under all synthetic conditions tested including acidic conditions (see chemistry section) and no epimerization was observed.

Addressing the Phe19 pocket. With a stable scaffold now in hand we then focused on increasing the binding affinity of our compounds to MDM2. Since no X-ray co-crystal structures of the new weakly potent undecorated compounds could be obtained we started our optimization based on docking results (e.g. Figure 2A) and biochemical measurements. We

first evaluated the influence of substituents in R¹ position of the pyrrolidine ring (Figure 1) to evaluate if additional polar interactions (e.g. His73, Tyr67) can be addressed or if potentially the Phe19 pocket can be occupied by using this vector. Lipophilic substituents like the benzyl group of **rac 5d** and others (shown in Table 1) only showed moderate improvement in potency and therefore the attempt of addressing the Phe19 pocket from this position was not further pursued. Installing side chains to address polar interactions as well resulted in only a moderate improvement of the IC₅₀ values by a factor of 2-3 compared to the unsubstituted compound **rac 5a** as shown for the racemic compounds **5g-5k** in Table 1. The only exception was compound **rac 5f** with a (1*H*-1,2,4-triazol-1-yl)methyl side-chain that led to an improvement by a factor of seven [IC₅₀ (MDM2-p53) = 5,502 nM] compared to **rac 5a**. No X-ray structure of **5f** in MDM2 could be obtained to help to understand the improved potency and we subsequently combined this beneficial R¹ side chain with substituents on the pyrrolidine nitrogen (*vide infra*).

In parallel we attempted to address the Phe19 pocket by introducing various substituents to the pyrrolidine nitrogen (R² in Table 2). Small and branched alkyl chains like the methylcyclopropyl group in **6d** [IC₅₀ (MDM2-p53) = 563 nM] led to a dramatic improvement in potency and to IC₅₀ values below 1 μM as shown for compounds **6a-d**. For this series predominantly compounds with a methyl group in R¹ have been prepared due to the better synthetic accessibility (see chemistry section). The compounds with methyl groups in R¹ showed very comparable potency to the corresponding compounds with hydrogen in R¹ as shown for the compound pair **5a** and **5b** (Table 1). Preparation of additional analogs led to further improvement of potency by a factor of five especially when a 3-ethoxy-benzyl substituent was introduced as shown for compound **6g**. Additionally the introduction of a fluorine atom in R³ to occupy the Leu26 pocket with the 3-chloro-2-fluorophenyl substituent gave an additional improvement in potency of a factor of up to four as shown for compound pair **6d** and **6e** (Table 2). Chiral separation of the racemic mixtures by chiral SFC showed a

clear eutomer/distomer behavior and the potency generally improved by a factor of two when comparing the racemate of a compound to its eutomer. This factor was demonstrated for racemate **rac 6g** ($IC_{50} = 57$ nM) and the eutomer **6g** ($IC_{50} = 34$ nM) while the distomer was 150 fold less potent.

The presumed binding mode from docking was confirmed by X-ray crystal structures of **6b** and **6g** bound to MDM2 (Figure 2) with the 3-chloro-phenyl for **6b** (respectively 2-fluoro-3-chloro phenyl for **6g**) deeply buried in the Leu26 pocket forming a key π - π interaction with His96, and with the 6-chloro-indolinone substituent binding to the Trp23 pocket forming a crucial hydrogen bond with its nitrogen proton to the backbone carbonyl of Leu54. For compound **6b** the neopentyl group binds to the Phe19 pocket as expected, but strikingly the 3-ethoxy benzyl substituent of compound **6g** induces a change in the protein conformation which leads to a larger Phe19 pocket compared to the crystal structure of **6b** mainly caused by the new orientation of the Trp67 side chain. This additional hydrophobic cleft was to the best of our knowledge observed the first time in an X-ray co-crystal structure with a spiro-oxindole compound and is filled ideally by the 3-ethoxy-phenyl substituent explaining the boost in potency (Figure 2 C and D).

The installation of a Phe19-pocket substituent to the most potent analog that came out of the R^1 screen (**rac 5f**, Table 1), carrying a (1*H*-1,2,4-triazol-1-yl)methyl substituent unfortunately did not show a further improvement in potency as shown in Table 2 (**rac 6f**). This fact is interesting since it is indicating that the (1*H*-1,2,4-triazol-1-yl)methyl substituent might also bind to the Phe19 pocket and could compete with the isopentyl group of **rac 6f**.

Addressing His96 and Lys94. To further improve potency we aimed to address the side chain of His96 with a hydrogen bond and therefore installed various groups offering hydrogen bond acceptors in R^4 . Neither the introduction of an amide (Table 3), nor other functional groups led to a significant improvement in potency suggesting that the compounds have the

wrong conformation to address His96 from R⁴. Compound **9** with a -CH₂CO₂H group at R⁴ led to a moderate improvement in potency with an IC₅₀ (MDM2-p53) of 62 nM compared to the 157 nM measured for compound **6e** with no substituent in R⁴. Attempts to address Lys94 from this scaffold with benzoic acid analog **2** also did not show significantly improved potency. We concluded this avenue of optimization assuming that the vectors to address directed polar interactions were not suitable.

Precise spatial positioning of atoms and functional groups is crucial for pharmacophore optimization of small molecule inhibitors and in particular for their directed polar interactions with proteins. Natural products utilize multiple fused rings not only to precisely position atoms and functional groups but also to reduce the degrees of freedom and possible conformations of biologically active molecules. Such complex natural product architectures as Spirotryprostatin B (Scheme 3) served as an inspiration to our design of a rigidified scaffold. By linking the free -NH₂ with the sidechain at the 2-position of the pyrrolidine we generated an octahydro-pyrrolo[3,2-b]pyrrole ring system (Scheme 3) which offered vectors better suited to address His96 and Leu94 with additional substituents.⁵⁸

The unsubstituted octahydro-pyrrolo[3,2-b]pyrrole compound **10** (R⁴ = H, Table 4) showed no improvement in potency compared to analogs **6e** and **8** respectively. However, attaching a -CH₂CO₂H group at R⁴ already led to a clearly improved IC₅₀ (MDM2-p53) of 39 nM. When we combined this beneficial substituent with the 3-ethoxy phenyl substituent in R² as a Phe-19-pocket substituent we observed an additional increase in potency to an IC₅₀ (MDM2-p53) of 2 nM for the enantiomerically pure compound **13**. An X-ray crystal structure of des-fluoro analog **14** in MDM2 (Figure 3) showed that the carboxylic acid substituent indeed forms a hydrogen bond interaction with the sidechain of His96 and Lys94 as intended and structurally explains the increased potency. Interestingly, the two amino acids His96 and Lys94 both adopted a new conformation compared to the structures obtained thus far (Figure 2). This new

protein conformation displayed a suboptimal π - π interaction of the His96 side chain with the Leu-pocket substituent (Figure 3B) and also displayed an energetically unfavorable bent conformation of the Lys94 side chain. We therefore searched for substituents in position R⁵ (Table 5) which would address Lys94 in its low-energy extended conformation (as observed in most X-ray co-crystal structures) and would allow ideal π - π interaction with the His96.

Compounds with 4-phenyl-CO₂H as R⁵ displayed a dramatic improvement in potency with an IC₅₀ (MDM2-p53) of 4 nM for compound **3** (BI-0252) with a cyclopropyl substituent in R². Compared to compound **2** we gained a factor of 27 in potency by formally only adding one bond and thereby locking the molecule in an ideal conformation for the interaction with the MDM2 protein (Scheme 4). Using the 3-ethoxy-phenyl substituent to address the Phe19 pocket gave compound **17** with an IC₅₀ (MDM2-p53) of 2 nM which is a factor of two more potent in this assay suggesting that at this point the assay-wall of the biochemical assay was reached. In the X-ray co-crystal structure of **3** in MDM2 (Figure 4) we did not observe any direct interaction of the benzoic acid substituent and the amino group of Lys94 although the groups are in close proximity. However, the pyrrolidine NH of **3** indeed forms an H-bond with the sidechain of His96 in this case with the N1-H tautomeric form of the imidazole as opposed to the N3-H tautomer observed in all interactions thus far. In addition the important π - π interaction with His96 now shows an ideal orientation in contrast to compound **14** (Figure 4B).

Cellular Potency and Selectivity. Selected compounds were tested for their cellular potency in the p53 wild type osteosarcoma SJSA-1 cell line proliferation assay (Table 6). Fully decorated compounds with biochemical IC₅₀ values below 10 nM showed strong cellular potency with **17** being the most potent compound of this series with 67 nM in the SJSA-1 assay. To assess the selectivity we tested the same set of compounds against the p53 mutant cell line SK-OV-3. Indicative of truly selective MDM2-p53 PPI inhibitors all compounds

tested showed no effect on the growth of the p53 mutant SK-OV-3 cell line up to a concentration of 25 μ M.

Pharmacokinetic Properties in Mice of 3, 16 and 17. Selected compounds were tested for their *in vivo* pharmacokinetic properties in non-tumor-bearing female NMRI nude mice. Single administration *iv* and *po* PK experiments were performed at an *iv* dose of 5 mg/kg and a *po* dose of 50 mg/kg for compounds **3**, **16** and **17**. Respective *iv* and *po* PK profiles are shown in Figure 5 and the derived mean PK parameters are listed in Table 7.

While compounds **3** and **16** show low clearance *in vivo* after *iv* administration, compound **17** shows a comparably high clearance and a rapid decay in plasma concentration. After *po* administration compound **3** shows the highest and compound **17** the lowest AUC value (Table 7). Compound **3** was selected for investigation in xenograft models due to its combined high *po in vivo* exposure and good cellular potency.

Single Dose Efficacy of 3 in a SJSA-1 Osteosarcoma Xenograft Model. *In vivo* efficacy of compound **3** was tested in the SJSA-1 osteosarcoma xenograft model (Figure 6). Compound **3** was administered orally at a daily dose of 25 mg/kg or at a single dose of 100 mg/kg. Regressions in all tumors were observed with compound **3** for both dose schedules showing that efficacy can be achieved with this compound using very different dose schedules. MDM2 inhibitors are expected to lead to TP53 accumulation and eventually induction of TP53 target genes. To confirm on-target activity of compound **3** *in vivo*, a PD biomarker study was performed in SJSA-1 tumor bearing mice. Tumors were harvested 6 and 24 hours after administering a single oral dose of 100 mg/kg. Target gene induction was measured using q-RT-PCR or Meso-Scale assays (Figure 6). Briefly, compound **3** leads to time-dependent mRNA induction of TP53 target genes including *CDKN1a*, *MDM2* and *BBC3* (Figure 6C). Meso-Scale assays confirm accumulation of TP53 and MDM2 protein as well as induction of cleaved CASPASE3, which is a PD biomarker of apoptosis (Figure 6D). In addition,

histological and immunohistochemical analysis was performed (Figure 7), which confirmed the findings by q-RT-PCR and Meso-Scale analysis. In summary, these results are in line with the mode of action of a MDM2 inhibitor and demonstrate that compound **3** acts as a MDM2 inhibitor.

To the best of our knowledge a single dose administration experiment in a mouse SJSA-1 xenograft model with a comparable result has only been reported by Wang et al at a dose of 200 mg/kg and was explained by the induction of apoptosis persisting for 72 hours.⁴⁷ Thrombocytopenia as an adverse event has been observed in clinical studies with several MDM2-p53 inhibitors. High grade thrombocytopenia occurred mostly when testing more continuous dose schedules with these inhibitors in the clinic (e.g. daily dosing for 5-10, 21 or 28 consecutive days per cycle)^{13, 59, 60}. More recent studies are testing less frequent dose schedules (e.g. once every 21 days)⁶¹ with the intention to manage thrombocytopenia as an on-target toxicity and it remains to be shown if this approach is successful. For future studies we plan to test this working hypothesis.

CHEMISTRY

The spiro[3H-indole-3,2'-pyrrolidin]-2(1H)-one core is constructed using a three component decarboxylative 1,3-dipolar cycloaddition of an isatin, an amino acid, and a nitrostyrene which generated the core structure with up to four stereocenters in racemic form in only a single step. The reaction gave moderate to good yields for the desired compounds in many cases but is strongly dependent on the nature of the amino acid component and produces regioisomers and diastereomers as byproducts in different ratios which was the subject of several theoretical^{62, 63} and experimental studies⁶⁴⁻⁶⁶. The selectivity favoring the desired product was completely reversed when glycine (lacking an amino acid sidechain) is used in the cycloaddition leading to the unwanted regioisomer **regio-5a** as the major product (48% isolated yield) while the desired compound **5a** was obtained in only 2%. Similar results were reported for the use of sarcosine as the amino acid component.⁶⁷ The reaction gave

significantly better yields for most analogs with larger substituents R^1 ($R^1 \neq H$) as summarized in Table 8.⁶⁶ For most examples minor amounts of additional isomers to **5** and **regio-5a** have been observed but were not further analyzed.

Compounds **6a-g** were prepared by reductive aminations of the cycloaddition products with the corresponding aldehydes followed by reduction of the nitro groups with In/HCl or Raney Nickel and H_2 in good yields (Scheme 5). The racemates of compounds **6** have been separated by chiral SFC for compounds **6a, b, d, e, g**.

Compound **8** was prepared from amine **6e** by amidation with HATU and acetic acid, while compounds **9** and **2** were prepared by a reductive amination with glyoxylic acid ethylester and methyl 4-formylbenzoate respectively followed by saponification with NaOH (Scheme 6).

Compound **10** could be prepared from intermediate **rac 5m** by reductive amination with cyclopropylcarboxaldehyde and sodium triacetoxyborohydride followed by reduction of the nitro group with indium powder and HCl and an intramolecular Mitsunobu reaction to generate the octahydro-pyrrolo[3,2-b]pyrrole ring system and chiral separation by SFC. Analogs **11-13** were prepared by reduction of compound **rac 5 m** with Raney Nickel and H_2 followed by a Mitsunobu reaction to give the common intermediate **rac 18**. Selective acetylation of the sterically less hindered pyrrolidine nitrogen followed by reductive amination gave compound **rac 11**. A reaction sequence starting with a selective reductive amination of **rac 18** and glyoxylic acid ethyl ester and subsequent reductive amination of the remaining secondary amine with cyclopropylcarboxaldehyde or 3-ethoxybenzaldehyde and final saponification delivered analogs **rac 12** and **13** respectively after chiral separation (Scheme 7).

The synthesis of compounds **3** and **16** (Scheme 8) commenced with reductive aminations of compound **rac 5m** with cyclopropylcarboxaldehyde or 3-ethoxybenzaldehyde respectively

1
2
3 followed by oxidations with IBX to the corresponding aldehydes **19** and **20**. Installation of the
4 benzoic acid motive was accomplished by iodine-magnesium exchange of 4-iodo-benzoic
5 acid esters **21** or **22** with *i*-PrMgCl·LiCl and subsequent Grignard addition to aldehydes **19**
6 and **20** to give the corresponding benzylic alcohols as a mixtures of two diastereomers
7 favoring the unwanted stereoisomers **23a** and **24a** (3.5 : 1 for **23a** : **23b** and 4.5 : 1 for **24a** :
8 **24b**).^{68, 69} The diastereomers were separated and oxidation of **23a** and **24a** to the ketones **25**
9 and **26** followed by reduction with NaBH₄ gave mixtures of diastereomers favoring the
10 desired compounds **23b** and **24b** (1 : 1.3 for **23a** : **23b** and 1 : 2.4 for **24a** : **24b**). Reducing the
11 nitro groups of **23b** with Raney Nickel and H₂ and of **24b** with indium and HCl, respectively
12 gave the corresponding primary amines which were used in intramolecular Mitsunobu
13 reactions to give compounds **14** and **27**. Saponification of these analogs delivered compounds
14 **3** and **16**. Amidation of **3** with ammonia and HATU gave the primary amide **15**.
15
16
17
18
19
20
21
22
23
24
25
26
27
28
29

30 DISCUSSION AND CONCLUSIONS

31
32
33 Inspired by Wang's spiroindolinone inhibitors^{31, 42} and natural product architectures we were
34 able to generate highly potent, selective and chemically stable MDM2-p53 PPI inhibitors. The
35 installation of a multiply fused ring system allowed the precise positioning of functional
36 groups for optimal hydrogen bond and π - π interactions leading to compounds with the above-
37 mentioned desired properties. As shown for compound **3**, tumor regressions in all animals of a
38 mouse SJSA-1 xenograft study have been achieved - even with a single dose of compound **3**,
39 with concomitant induction of TP53 target genes and markers of apoptosis.
40
41
42
43
44
45
46
47
48

49
50 High grade thrombocytopenia was reported for MDM2-p53 PPI inhibitors as an adverse event
51 in the clinic in particular when testing continuous dose schedules. For future studies we plan
52 to test less frequent dose schedules with the intention to manage thrombocytopenia as an on-
53 target toxicity.
54
55
56
57
58
59
60

EXPERIMENTAL SECTION

Unless otherwise indicated all reactions were carried out in standard commercially available glassware using standard synthetic chemistry methods. Air-sensitive and moisture-sensitive reactions were performed under an atmosphere of dry nitrogen or argon with dried glassware. Commercial starting materials were used without further purification. Solvents used for reactions were of commercial “dry”- or “extra-dry” or “analytical” grade. All other solvents used were reagent grade. Preparative RP-HPLC was carried out on Agilent or Gilson systems using columns from Waters (Sunfire C18 OBD, 5 or 10 μ m, 20x50 mm, 30x50 mm or 50x150 mm; X-Bridge C18 OBD, 5 or 10 μ m, 20x50, 30x50, or 50x150 mm) or YMC (Triart C18, 5 or 10 μ m, 20x50 mm, or 30x50 mm). Unless otherwise indicated compounds were eluted with MeCN/water gradients using either acidic (0.2 % HCOOH or TFA) or basic water (5 mL 2 M NH_4HCO_3 + 2 mL NH_3 (32 %) made up to 1 L with water).

NMR experiments were recorded on Bruker Avance 400 MHz and 500 MHz spectrometers at 298K. Samples were dissolved in 600 μ L DMSO- d_6 and TMS was added as an internal standard. 1D ^1H spectra were acquired with 30° excitation pulses and an interpulse delay of 4.2sec with 64k datapoints and 20ppm sweep width. 1D ^{13}C spectra were acquired with broadband composite pulse decoupling (WALTZ16) and an interpulse delay of 3.3sec with 64k datapoints and a sweep width of 240ppm. Processing and analysis of 1D spectra was performed with Bruker Topspin 3.0 software. No zero filling was performed and spectra were manually integrated after automatic baseline correction.

HPLC-MS: All samples were analyzed on an Agilent 1100 series LC system coupled with an Agilent 6140 mass spectrometer. Purity was determined via UV detection with a bandwidth of 170nm in the range from 230-400nm. LC parameters were as follows: Waters Xbridge C18 column, 2.5 μ m particle size, 2.1 x 20mm. Run time 2.1 minutes, flow 1ml/min, column temperature 60°C and 5 μ L injections. Solvent A (20mM NH_4HCO_3 / NH_3 pH 9), solvent B (MS grade acetonitrile). Start 10% B, gradient 10% - 95% B from 0.0 - 1.5min, 95% B from

1.5 - 2.0min, gradient 95% - 10% B from 2.0 – 2.1min. HRMS data were recorded using a Thermo Scientific Orbitrap Elite hybrid ion trap/orbitrap spectrometer system with an Ultimate 3000 series LPG-3400XRS pump system. Mass calibration was performed using the Pierce LTQ Velos ESI positive ion calibration solution from Thermo Scientific (lot PF200011, product no. 88323). All biologically evaluated compounds exist in >95% purity as shown by LC/MS, additionally for **3**, **16** and **17** purity > 95% was shown by Q-NMR.

Chiral separation by SFC: The separations were carried out on a JASCO SFC-system under isocratic conditions. The system is equipped with a CO₂-pump PU2088 and a cosolvent pump PU2086. The sample is injected by an autosampler AS2059SF, the signal is detected by an UV-detector UV2075 and the backpressure (150bar) was regulated by the BP2080. The fractions were collected by a fraction-collector FC2088-08. Mobile phase was CO₂ (Air Liquide, Schwechat) and methanol (Merck, Darmstadt). Chromatographic separation was obtained by isocratic conditions using several chiral columns (250x20mm; 5µm) from Daicel (Strasbourg, Europe) at 40°C a flow of 50 mL/min. Inside the chiral columns are chiral resolving agents based on cellulose or amylose. Docking Studies: GOLD Suite v 5.4 from CCDC Software Limited was used for the docking of compound **5B** (Figure 2). Hydrogen bonding to the backbone carbonyl oxygen of Leucine 54 was defined as the constraints during the docking process. Ligands were prepared using CORINA prior to the docking.

Selected Experimental Procedures

Synthesis of Compound 3:

4-[(3S,3'S,3'aS,5'R,6'aS)-6-chloro-3'-(3-chloro-2-fluorophenyl)-1'-(cyclopropylmethyl)-2-oxo-1,2,3',3'a,4',5',6',6'a-octahydro-1'H-spiro[indole-3,2'-pyrrolo[3,2-b]pyrrole]-5'-yl]benzoic acid (3)

To a solution of compound **14** (150 mg, 0.258 mmol) in THF (5 mL) was added NaOH (97 μ L, 8 M in H₂O) and the reaction mixture was stirred at 60 °C for 18 h. The reaction mixture was concentrated *in vacuo* and the crude product was purified by preparative RP HPLC (Gilson, gradient 10-55% MeCN in H₂O) to give compound **3**. 4-[(3*S*,3'*S*,3'a*S*,5'*R*,6'a*S*)-6-chloro-3'-(3-chloro-2-fluorophenyl)-1'-(cyclopropylmethyl)-2-oxo-1,2,3',3'a,4',5',6',6'a-octahydro-1'H-spiro[indole-3,2'-pyrrolo[3,2-b]pyrrole]-5'-yl]benzoic acid (**3**) (131 mg, 0.231 mmol, 90%). ¹H NMR (500 MHz, DMSO-*d*₆) δ ppm -0.16 (dq, *J*=9.46, 4.73 Hz, 1 H) 0.00 (dq, *J*=9.46, 4.73 Hz, 1 H) 0.23 (tt, *J*=8.75, 4.65 Hz, 1 H) 0.36 (tt, *J*=8.59, 4.65 Hz, 1 H) 0.61 - 0.71 (m, 1 H) 1.55 - 1.64 (m, 1 H) 2.03 (dd, *J*=12.61, 7.88 Hz, 1 H) 2.21 (dd, *J*=12.45, 5.83 Hz, 1 H) 2.37 (dd, *J*=12.29, 5.36 Hz, 1 H) 3.89 (d, *J*=9.14 Hz, 1 H) 4.02 (t, *J*=7.41 Hz, 1 H) 4.52 (dd, *J*=10.88, 5.20 Hz, 1 H) 4.66 (t, *J*=8.35 Hz, 1 H) 6.55 (d, *J*=1.89 Hz, 1 H) 7.04 (dd, *J*=7.88, 1.89 Hz, 1 H) 7.13 (t, *J*=8.04 Hz, 1 H) 7.31 - 7.36 (m, 1 H) 7.43 - 7.47 (m, 2 H) 7.49 (d, *J*=8.20 Hz, 2 H) 7.84 (d, *J*=8.20 Hz, 2 H) 10.21 (br s, 1 H); ¹³C NMR (126 MHz, DMSO-*d*₆) δ ppm 3.92, 5.99, 11.41, 45.03, 49.73, 55.59, 59.62, 66.61, 67.85, 78.10, 109.73, 119.73 (d, *J*_{C-F}=19.98 Hz), 122.19, 125.41 (d, *J*_{C-F}=4.54 Hz), 126.02 (d, *J*_{C-F}=13.62 Hz), 126.13, 127.37, 127.39, 128.77, 129.65, 129.70, 133.58, 144.00, 156.69 (d, *J*_{C-F}=247.04 Hz) 178.33; HRMS (ESI⁺): calculated for C₃₀H₂₆Cl₂FN₃O₃ [M+H]⁺ 566.14080, found 566.14246, Δ 2.93 ppm; LC/MS: [M+H]⁺ = 566; t_R = 1.06 min.

Rac-(3*S*,3'*S*,4'*S*,5'*S*)-6-chloro-3'-(3-chloro-2-fluorophenyl)-5'-(2-hydroxyethyl)-4'-nitro-1,2-dihydrospiro[indole-3,2'-pyrrolidine]-2-one (**rac 5m**)

6-Chloroisatin (8.0 g, 44.05 mmol), 1-(2-fluoro-3-chlorophenyl)-2-nitroethene (8.9 g, 44.05 mmol) and L-homoserin (5.24 g, 44.05 mmol) were stirred under reflux in MeOH (10 mL) for 18 h. The reaction mixture was concentrated *in vacuo* and the residue titrated in acetonitrile. The solid was filtered and dried to give **rac 5m** which was used in the next step without further purification. *Rac*-(3*S*,3'*S*,4'*S*,5'*S*)-6-chloro-3'-(3-chloro-2-fluorophenyl)-5'-(2-

hydroxyethyl)-4'-nitro-1,2-dihydrospiro[indole-3,2'-pyrrolidine]-2-one (**rac 5m**) (8.9 g, 20.2 mmol, 46%). ¹H NMR (500 MHz, DMSO-*d*₆) δ ppm 1.49 - 1.63 (m, 2 H) 3.44 - 3.52 (m, 1 H) 3.52 - 3.61 (m, 1 H) 4.09 (d, *J*=7.25 Hz, 1 H) 4.52 - 4.63 (m, 2 H) 4.74 (d, *J*=8.51 Hz, 1 H) 6.06 (t, *J*=8.51 Hz, 1 H) 6.66 (s, 1 H) 7.11 (dd, *J*=7.88, 0.95 Hz, 1 H) 7.17 (t, *J*=7.88 Hz, 1 H) 7.44 (br t, *J*=6.94 Hz, 2 H) 7.56 (d, *J*=7.88 Hz, 1 H) 10.32 (s, 1 H); LC/MS: [M+H]⁺ = 440; *t*_R = 1.21 min.

Methyl 4-[(3S,3'S,3'aS,5'R,6'aS)-6-chloro-3'-(3-chloro-2-fluorophenyl)-1'-(cyclopropylmethyl)-2-oxo-1,2,3',3'a,4',5',6',6'a-octahydro-1'H-spiro[indole-3,2'-pyrrolo[3,2-b]pyrrole]-5'-yl]benzoate (14)

A solution of intermediate **23b** (830 mg, 1,321 mmol) in MeOH (10 mL) and DCM (8 mL) was stirred in Büchi laboratory autoclave with Raney Ni (78 mg) under a H₂ pressure of 8 bar for 18 h at room temperature. The Raney Ni was filtered off carefully and the solvent removed in vacuo. The crude product was purified by preparative RP HPLC (Gilson, 40-85 % MeCN in H₂O) to give methyl 4-[(1R)-2-[(3S,3'S,4'S,5'S)-4'-amino-6-chloro-3'-(3-chloro-2-fluorophenyl)-1'-(cyclopropylmethyl)-2-oxo-1,2-dihydrospiro[indole-3,2'-pyrrolidine]-5'-yl]-1-hydroxyethyl]benzoate (593 mg, 0.990 mmol, 75%). ¹H NMR (500 MHz, DMSO-*d*₆) δ ppm -0.28 - -0.21 (m, 1 H) -0.04 - 0.05 (m, 1 H) 0.08 - 0.17 (m, 1 H) 0.25 - 0.32 (m, 1 H) 0.45 - 0.53 (m, 1 H) 1.99 (br d, *J*=14.50 Hz, 1 H) 2.14 - 2.19 (m, 1 H) 2.20 - 2.24 (m, 1 H) 2.25 - 2.29 (m, 1 H) 2.25 - 2.29 (m, 1 H) 2.35 (br d, *J*=8.51 Hz, 1 H) 2.46 - 2.48 (m, 1 H) 3.58 (br t, *J*=8.35 Hz, 1 H) 3.75 (d, *J*=11.35 Hz, 1 H) 3.79 (s, 2 H) 4.52 - 4.60 (m, 1 H) 4.80 (dd, *J*=10.72, 2.52 Hz, 1 H) 6.49 (d, *J*=1.89 Hz, 1 H) 6.98 (dd, *J*=7.88, 1.89 Hz, 1 H) 7.11 (t, *J*=7.88 Hz, 1 H) 7.21 (d, *J*=7.88 Hz, 1 H) 7.30 - 7.37 (m, 2 H) 7.49 (d, *J*=8.51 Hz, 1 H) 7.47 - 7.53 (m, 1 H) 7.88 (d, *J*=8.20 Hz, 1 H) 7.86 - 7.89 (m, 1 H) 7.87 - 7.90 (m, 1 H) 10.09 (s, 1 H). LC/MS: [M+H]⁺ = 598; *t*_R = 1.48 min. To a solution of methyl 4-[(1R)-2-[(3S,3'S,4'S,5'S)-4'-amino-6-chloro-3'-(3-chloro-2-fluorophenyl)-1'-(cyclopropylmethyl)-2-oxo-1,2-dihydrospiro[indole-3,2'-pyrrolidine]-5'-yl]-1-hydroxyethyl]benzoate (213 mg, 0.356 mmol)

in DCM (4 mL) was added triphenylphosphine (102 mg, 0.39 mmol) and DEAD (195 μ L, 0.43 mmol, 40 % in toluene) and the reaction mixture was stirred for 18 h at rt. Saturated aqueous NaHCO₃ solution was added to the reaction mixture and the mixture was extracted with DCM. The combined organic layer was dried (MgSO₄), filtered, concentrated *in vacuo* and the crude product was purified by preparative RP HPLC (Gilson, gradient 50-90% MeCN in H₂O) to give methyl 4-[(3S,3'S,3'aS,5'R,6'aS)-6-chloro-3'-(3-chloro-2-fluorophenyl)-1'-(cyclopropylmethyl)-2-oxo-1,2,3',3'a,4',5',6',6'a-octahydro-1'H-spiro[indole-3,2'-pyrrolo[3,2-b]pyrrole]-5'-yl]benzoate (**14**) (55 mg, 0.267 mmol, 75%). ¹H NMR (500 MHz, DMSO-*d*₆) δ ppm -0.16 (dq, *J*=9.46, 4.73 Hz, 1 H) 0.01 (dq, *J*=9.46, 4.73 Hz, 1 H) 0.23 (tt, *J*=8.75, 4.65 Hz, 1 H) 0.32 - 0.40 (m, 1 H) 0.61 - 0.70 (m, 1 H) 1.59 (td, *J*=11.74, 6.78 Hz, 1 H) 2.03 (dd, *J*=12.45, 7.72 Hz, 1 H) 2.21 (dd, *J*=12.45, 5.83 Hz, 1 H) 2.37 (dd, *J*=12.29, 5.36 Hz, 1 H) 2.92 (br dd, *J*=8.98, 3.94 Hz, 1 H) 3.80 (s, 3 H) 3.89 (d, *J*=9.14 Hz, 1 H) 4.02 (t, *J*=7.41 Hz, 1 H) 4.50 - 4.58 (m, 1 H) 4.66 (td, *J*=8.28, 3.63 Hz, 1 H) 6.54 (d, *J*=1.89 Hz, 1 H) 7.04 (dd, *J*=7.88, 1.89 Hz, 1 H) 7.13 (s, 1 H) 7.31 - 7.37 (m, 1 H) 7.41 - 7.48 (m, 2 H) 7.54 (d, *J*=8.51 Hz, 2 H) 7.87 (d, *J*=8.51 Hz, 2 H) 10.20 (s, 1 H); LC/MS: [M+H]⁺ = 580; *t*_R = 1.59 min.

2-[(3S,3'S,4'S,5'S)-6-chloro-3'-(3-chloro-2-fluorophenyl)-1'-(cyclopropylmethyl)-4'-nitro-2-oxo-1,2-dihydrospiro[indole-3,2'-pyrrolidine]-5'-yl]acetaldehyde (**19**)

To a solution of cyclopropylcarboxaldehyde (508 μ L, 6.81 mmol) in DMF (2 mL) was added intermediate **rac 5m** (1.0 g, 2.27 mmol) and AcOH (2.6 mL, 45.43 mmol) and the reaction mixture was stirred for 15 min at room temperature. Sodium triacetoxyborohydride (1.52 g, 6.81 mmol) was added and the reaction mixture was stirred for 18 h. Water was added to the reaction mixture and it was extracted with EtOAc. The combined organic layer was dried (MgSO₄), filtered, concentrated *in vacuo* to give rac-(3S,3'S,4'S,5'S)-6-chloro-3'-(3-chloro-2-fluorophenyl)-1'-(cyclopropylmethyl)-5'-(2-hydroxyethyl)-4'-nitro-1,2-dihydrospiro[indole-

3,2'-pyrrolidine]-2-one (1.03 g, 2.078 mmol, 92%) which was separated by chiral SFC to obtain (3S,3'S,4'S,5'S)-6-chloro-3'-(3-chloro-2-fluorophenyl)-1'-(cyclopropylmethyl)-5'-(2-hydroxyethyl)-4'-nitro-1,2-dihydrospiro[indole-3,2'-pyrrolidine]-2-one (>95% ee). ¹H NMR (400 MHz, DMSO-*d*₆) δ ppm -0.20 (dt, *J*=9.57, 4.72 Hz, 1 H) 0.01 (dq, *J*=9.44, 4.88 Hz, 1 H) 0.09 - 0.18 (m, 1 H) 0.23 - 0.33 (m, 1 H) 0.45 - 0.57 (m, 1 H) 1.77 (dq, *J*=13.91, 6.69 Hz, 1 H) 1.92 - 2.02 (m, 1 H) 2.31 (dd, *J*=13.69, 7.10 Hz, 1 H) 2.58 - 2.64 (m, 1 H) 3.54 - 3.68 (m, 2 H) 4.21 (ddd, *J*=9.50, 6.84, 4.94 Hz, 1 H) 4.71 (t, *J*=4.94 Hz, 1 H) 4.78 (d, *J*=11.41 Hz, 1 H) 6.42 (dd, *J*=11.28, 9.76 Hz, 1 H) 6.69 (d, *J*=1.77 Hz, 1 H) 7.19 (dd, *J*=7.98, 1.90 Hz, 1 H) 7.23 (t, *J*=7.98 Hz, 1 H) 7.43 - 7.49 (m, 1 H) 7.51 - 7.56 (m, 1 H) 7.56 - 7.60 (m, 1 H) 7.57 (d, *J*=8.11 Hz, 1 H) 10.57 (s, 1 H); LC/MS: [M+H]⁺ = 494; *t*_R = 1.39 min. To a solution of (3S,3'S,4'S,5'S)-6-chloro-3'-(3-chloro-2-fluorophenyl)-1'-(cyclopropylmethyl)-5'-(2-hydroxyethyl)-4'-nitro-1,2-dihydrospiro[indole-3,2'-pyrrolidine]-2-one (1.00 g, 2.02 mmol) in CH₃CN (13 mL) was added IBX (680 mg, 2.43 mmol) and the reaction mixture was stirred for 60 min at 75 °C. The reaction mixture was cooled to 0 °C and kept at this temperature for 1 h without stirring before it was filtered through Celite® and concentrated *in vacuo*. The crude product was used without further purification for the next step. 2-[(3S,3'S,4'S,5'S)-6-chloro-3'-(3-chloro-2-fluorophenyl)-1'-(cyclopropylmethyl)-4'-nitro-2-oxo-1,2-dihydrospiro[indole-3,2'-pyrrolidine]-5'-yl]acetaldehyde (**19**) (926 mg, 1.88 mmol, 93%). ¹H NMR (400 MHz, DMSO-*d*₆) δ ppm -0.01 (dq, *J*=9.38, 4.73 Hz, 1 H) 0.18 (dq, *J*=9.38, 4.73 Hz, 1 H) 0.34 - 0.42 (m, 1 H) 0.43 - 0.54 (m, 1 H) 0.65 - 0.77 (m, 1 H) 2.38 - 2.48 (m, 1 H) 2.52 - 2.60 (m, 1 H) 3.08 - 3.17 (m, 1 H) 3.19 - 3.28 (m, 1 H) 4.83 (td, *J*=8.93, 3.17 Hz, 1 H) 4.98 (d, *J*=11.15 Hz, 1 H) 6.58 (t, *J*=10.27 Hz, 1 H) 6.85 (d, *J*=1.77 Hz, 1 H) 7.34 (dd, *J*=8.11, 1.77 Hz, 1 H) 7.38 (t, *J*=8.11 Hz, 1 H) 7.62 (br t, *J*=7.22 Hz, 1 H) 7.67 (br t, *J*=7.48 Hz, 1 H) 7.75 (d, *J*=7.86 Hz, 1 H) 9.94 (s, 1 H) 10.75 (s, 1 H); LC/MS: [M+H]⁺ = 492; *t*_R = 1.44 min.

Methyl 4-[(1R)-2-[(3S,3'S,4'S,5'S)-6-chloro-3'-(3-chloro-2-fluorophenyl)-1'-(cyclopropylmethyl)-4'-nitro-2-oxo-1,2-dihydrospiro[indole-3,2'-pyrrolidine]-5'-yl]-1-hydroxyethyl]benzoate (**23b**)

To a solution of methyl 4-iodobenzoate **21** (3.85 g, 14.381 mmol) in dry THF (15 mL) under argon atmosphere at - 40 °C was added isopropylmagnesium chloride lithium chloride complex (11.1 mL, 14.38 mmol, 1.3 M in THF) dropwise and the reaction mixture was stirred for 1 h. A solution of aldehyde **19** (2.36 mg, 4.79 mmol) in THF (40 mL) was added slowly at - 40 °C and the reaction mixture was stirred for 1.5 h and was slowly warmed to rt overnight. Water and Et₂O were added to the reaction mixture and the phases were separated. The aqueous phase was extracted with Et₂O and the combined organic layer was dried (MgSO₄), filtered, concentrated *in vacuo*. The crude product was purified by normal phase MPLC chromatography (10-22 % EtOAc in cyclohexane) to give compounds **23a** and **23b**. Methyl 4-[(1S)-2-[(3S,3'S,4'S,5'S)-6-chloro-3'-(3-chloro-2-fluorophenyl)-1'-(cyclopropylmethyl)-4'-nitro-2-oxo-1,2-dihydrospiro[indole-3,2'-pyrrolidine]-5'-yl]-1-hydroxyethyl]benzoate (**23a**) (1.92 g, 3,055 mmol, 64%). ¹H NMR (500 MHz, DMSO-*d*₆) δ ppm -0.19 (dq, *J*=9.42, 4.74 Hz, 1 H) -0.02 - 0.11 (m, 2 H) 0.17 - 0.26 (m, 1 H) 0.40 - 0.49 (m, 1 H) 1.73 - 1.82 (m, 1 H) 2.09 - 2.17 (m, 1 H) 2.51 (dd, *J*=13.87, 7.25 Hz, 1 H) 2.85 (dd, *J*=13.56, 5.99 Hz, 1 H) 3.96 (s, 3 H) 4.22 (td, *J*=8.51, 5.04 Hz, 1 H) 4.85 (d, *J*=11.66 Hz, 1 H) 4.93 - 5.01 (m, 1 H) 5.80 (d, *J*=4.73 Hz, 1 H) 6.53 (dd, *J*=11.66, 9.46 Hz, 1 H) 6.72 (d, *J*=1.89 Hz, 1 H) 7.23 - 7.31 (m, 2 H) 7.42 - 7.49 (m, 1 H) 7.54 - 7.60 (m, 1 H) 7.66 (d, *J*=8.20 Hz, 2 H) 7.75 (d, *J*=7.88 Hz, 1 H) 8.08 (d, *J*=8.20 Hz, 2 H) 10.59 (br s, 1 H); LC/MS: [M+H]⁺ = 628; *t*_R = 1.56 min. Methyl 4-[(1R)-2-[(3S,3'S,4'S,5'S)-6-chloro-3'-(3-chloro-2-fluorophenyl)-1'-(cyclopropylmethyl)-4'-nitro-2-oxo-1,2-dihydrospiro[indole-3,2'-pyrrolidine]-5'-yl]-1-hydroxyethyl]benzoate (**23b**) (532 mg, 0.846 mmol, 18%). ¹H NMR (500 MHz, DMSO-*d*₆) δ ppm -0.20 (dq, *J*=9.69, 4.76 Hz, 1 H) 0.01 (dq, *J*=9.62, 4.78 Hz, 1 H) 0.14 - 0.23 (m, 1 H) 0.27 - 0.36 (m, 1 H) 0.55 - 0.64 (m, 1 H) 1.91 (br dd, *J*=14.82, 9.46 Hz, 1 H) 2.09 - 2.22 (m, 2 H) 2.55 (d, *J*=1.89 Hz, 1 H) 3.88 (s, 3 H)

4.45 (t, $J=8.98$ Hz, 1 H) 4.67 (br dd, $J=10.09$, 4.10 Hz, 1 H) 4.87 (d, $J=11.03$ Hz, 1 H) 5.76 (d, $J=4.10$ Hz, 1 H) 6.44 - 6.50 (m, 1 H) 6.67 (d, $J=1.89$ Hz, 1 H) 7.14 (dd, $J=8.20$, 1.89 Hz, 1 H) 7.22 (t, $J=7.88$ Hz, 1 H) 7.42 (d, $J=8.20$ Hz, 2 H) 7.46 (t, $J=6.78$ Hz, 1 H) 7.48 - 7.53 (m, 1 H) 7.55 (d, $J=8.20$ Hz, 1 H) 7.98 (d, $J=8.20$ Hz, 2 H) 10.52 (br s, 1 H); LC/MS: $[M+H]^+ = 628$; $t_R = 1.61$ min. To a solution of **23a** (1.92 g, 3.06 mmol) in a MeCN (15 mL) was added IBX (984 mg, 3.51 mmol) and the reaction mixture was stirred for 2 hours at 75 °C. The reaction mixture was cooled to 0 °C and kept at this temperature for one hour without stirring before it was filtered through Celite® and concentrated in vacuo. The crude ketone **25** (1.76 g, 2.80 mmol, 92%) was used without further purification for the next step. To a solution of **25** (1.76 g, 2.80 mmol) in MeOH (10 mL) was slowly added sodium borohydride (106 mg, 2.80 mmol) at 0 °C and the reaction mixture was stirred at the same temperature for 6 h. The reaction mixture was quenched with water and saturated aqueous NaHCO₃ solution was added to the mixture. The aqueous phase was extracted with EtOAc and the combined organic layer was dried (MgSO₄), filtered, concentrated in vacuo. The crude product was purified by preparative RP HPLC (Gilson, gradient 50-90% MeCN in H₂O) to give compounds **23a** (630 mg, 1.002 mmol, 36%) and **23b**. 831 mg (1.322 mmol, 47%)

ASSOCIATED CONTENT

Supporting Information.

Synthesis procedures; method description for biochemical and cell proliferation assays; method description for *in vivo* studies and biomarker studies; Histopathological analyses and immunohistochemistry; NMR spectra; crystallographic data collection and refinement statistics (PDF); molecular formula string (CSV). This material is available free of charge on the ACS Publications website at <http://pubs.acs.org>.

Accession Codes

The atomic coordinates and structure factors have been deposited in the RCSB Protein Data Bank (compound **6b**: PDB code 5LAV; compound **6g**: PDB code 5LAY; compound **14**: PDB code 5LAW; and compound BI-0252 (**3**): PDB code 5LAZ). Authors will release the atomic coordinates and experimental data upon article publication.

AUTHOR INFORMATION

* corresponding author, email: andreas.gollner@boehringer-ingelheim.com

Phone: +43 (1) 80 105-2596

Notes

The authors declare the following competing financial interest: all authors were full Boehringer Ingelheim full-time employees at the time when this study was performed.

Boehringer-Ingelheim is grateful for financial support by the Austrian Research Promotion Agency FFG (grant: 832260, 837815 and 842856).

AUTHOR CONTRIBUTION

A.G. supervised the medicinal chemistry team, designed the compounds and synthetic strategies. A.G. and D.R. wrote the manuscript. G.D., P.E., A.G., C.K., J.Ra., H.W. T.W. contributed to the medicinal chemistry strategy and compound design. D.R. supervised the biology team and designed and supervised the animal experiments. G.B., D.R., R.S., U.W.-C., S.M.B. designed and supervised biological experiments, A.S. performed histopathological analyses and IHC. D.K. analysed the crystal structures. X-L.C. performed the docking studies. T.G. supervised the biochemical Alpha assays and cell proliferation assays. M.B. and J.K.-Oe. synthesized the compounds and developed the chemistry routes. J.Ri. supervised PK studies and wrote the PK section. H.A. supervised the HRMS measurements and chemical stability studies, D.B.McC. was responsible for the medicinal chemistry strategy and reviewed the manuscript.

ACKNOWLEDGMENTS

The authors thank Christoph Albrecht, Christian Aumeyer, Gerd Bader, Alexandra Beran, Helmut Berger, Christoph Burdack, Tuncay Ciftci, Ida Dinold, Nora Dürkop, Norbert Eidkum, Wolfgang Egermann, Gerlinde Flotzinger, Geraldine Garavel, Gerhard Gmaschitz, Gregor Grotemeier, Eric Haaksma, Petra Handler, Daniela Härnig, Wolfgang Hela, Cederic Kalinski, Matthew Kennedy, Matthias Klemencic, Michael Kulhanek, Roland Kousek, Norbert Kraut, Moriz Mayer, Katharina Mayr, Sabine Olt, Christina Puri, Alexander Wlachos, Christina Puri, Christoph Peinsipp, Oliver Petermann, Jens Quant, Carlos Roberto Ramirez-Santa Cruz, Maria Rieger, Günther Ross, Christian Salamon, Otmar Schaaf, Maike Scheller, Yvonne Scherbatin, Andreas Schrenk, Norbert Schweifer, Gorana Sijan, David Sill, Steffen Steurer, Michaela Streicher, Harald Studensky, Steffen Weik, Irene Weiner, Anika Weiss, Andreas Wernitznig, Alexander Wlachos, Susanne Wollner-Gaida, Markus Zeeb, and Andreas Zöphel

ABBREVIATIONS USED

1
2
3 BBC3, BCL2 binding component 3; BCL2, B-cell lymphoma 2, CL, clearance; *c*-Pr,
4 cyclopropyl; CDKN1*a*, Cyclin-Dependent Kinase Inhibitor 1A; DEAD, diethyl
5 azodicarboxylate; DIPEA, N,N-diisopropylethylamine; HATU, O-(7-Azabenzotriazol-1-yl)-
6 N,N,N',N'-tetramethyluronium-hexafluorophosphat; HCl, hydrochloric acid; HDM2, human
7 analogue of MDM2; HP- β -CD, 2-hydroxypropyl- β -cyclodextrin; IBX, 2-iodoxybenzoic acid;
8 In, indium; MDM2, murine double minute 2, MeCN, acetonitrile; NaOH, sodium hydroxide;
9 PhMe, toluene; PPI, protein-protein interaction; rac, racemic; RP-HPLC, reversed phase high-
10 performance liquid chromatography; Vss, volume of distribution steady state.
11
12
13
14
15
16
17
18
19
20
21
22
23
24
25
26
27
28
29
30
31
32
33
34
35
36
37
38
39
40
41
42
43
44
45
46
47
48
49
50
51
52
53
54
55
56
57
58
59
60

6b: PDB code 5LAV; compound **6g**: PDB code 5LAY; compound **14**: PDB code 5LAW; and compound BI-0252 (**3**): PDB code 5LAZ). Authors will release the atomic coordinates and experimental data upon article publication.

REFERENCES

1. Lane, D. P. p53, guardian of the genome. *Nature (London, U. K.)* **1992**, *358*, 15-16.
2. Levine, A. J.; Oren, M. The first 30 years of p53: growing ever more complex. *Nat. Rev. Cancer* **2009**, *9*, 749-758.
3. Kandoth, C.; McLellan, M. D.; Vandin, F.; Ye, K.; Niu, B.; Lu, C.; Xie, M.; Zhang, Q.; McMichael, J. F.; Wyczalkowski, M. A.; Leiserson, M. D. M.; Miller, C. A.; Welch, J. S.; Walter, M. J.; Wendl, M. C.; Ley, T. J.; Wilson, R. K.; Raphael, B. J.; Ding, L. Mutational landscape and significance across 12 major cancer types. *Nature (London, U. K.)* **2013**, *502*, 333-339.
4. Lawrence, M. S.; Stojanov, P.; Mermel, C. H.; Robinson, J. T.; Garraway, L. A.; Golub, T. R.; Meyerson, M.; Gabriel, S. B.; Lander, E. S.; Getz, G. Discovery and saturation analysis of cancer genes across 21 tumour types. *Nature (London, U. K.)* **2014**, *505*, 495-501.
5. Donehower, L. A.; Harvey, M.; Slagle, B. L.; McArthur, M. J.; Montgomery, C. A.; Butel, J. S.; Allan, B. Mice deficient for p53 are developmentally normal but susceptible to spontaneous tumours. *Nature (London, U. K.)* **1992**, *356*, 215-221.
6. Jones, S. N.; Roe, A. E.; Donehower, L. A.; Bradley, A. Rescue of embryonic lethality in Mdm2-deficient mice by absence of p53. *Nature (London, U. K.)* **1995**, *378*, 206-208.
7. Hu, W.; Feng, Z.; Levine, A. J. The regulation of multiple p53 stress responses is mediated through MDM2. *Genes Cancer* **2012**, *3*, 199-208.
8. Ventura, A.; Kirsch, D. G.; McLaughlin, M. E.; Tuveson, D. A.; Grimm, J.; Lintault, L.; Newman, J.; Reczek, E. E.; Weissleder, R.; Jacks, T. Restoration of p53 function leads to tumour regression in vivo. *Nature (London, U. K.)* **2007**, *445*, 661-665.

9. Xue, W.; Zender, L.; Miething, C.; Dickins, R. A.; Hernando, E.; Krizhanovsky, V.; Cordon-Cardo, C.; Lowe, S. W. Senescence and tumour clearance is triggered by p53 restoration in murine liver carcinomas. *Nature (London, U. K.)* **2007**, *445*, 656-660.
10. Martins, C. P.; Brown-Swigart, L.; Evan, G. I. Modeling the therapeutic efficacy of p53 restoration in tumors. *Cell* **2006**, *127*, 1323-1334.
11. Zhao, Y.; Bernard, D.; Wang, S. Small molecule Inhibitors of MDM2-p53 and MDMX-p53 interactions as new cancer therapeutics. *BioDiscovery* **2013**, *8*, 4.
12. Iancu-Rubin, C.; Mosoyan, G.; Glenn, K.; Gordon, R. E.; Nichols, G. L.; Hoffman, R. Activation of p53 by the MDM2 inhibitor RG7112 impairs thrombopoiesis. *Exp. Hematol. (N. Y., NY, U. S.)* **2014**, *42*, 137-145.e5.
13. Siu, L.; Italiano, A.; Miller, W. H.; Blay, J.-Y.; Gietema, J. A.; Bang, Y.-J.; Mileschkin, L. R.; Hirte, H. W.; Reckner, M.; Higgins, B.; Jukofsky, L.; Blotner, S.; Zhi, J.; Middleton, S.; Nichols, G. L.; Chen, L. C. Phase 1 dose escalation, food effect, and biomarker study of RG7388, a more potent second-generation MDM2 antagonist, in patients (pts) with solid tumors. *J. Clin. Oncol.* 2014, *32*, 5s, (Suppl; Abstr 2535), 32.
14. Wagner, A. J.; Banerji, U.; Mahipal, A.; Somaiah, N.; Hirsch, H. A.; Fancourt, C.; Levonas, A.; Lam, R.; Meister, A.; Kemp, R. K.; Knox, C.; Rose, S.; Hong, D. S. A phase I trial of the human double minute 2 (HDM2) inhibitor MK-8242 in patients (pts) with advanced solid tumors. *J. Clin. Oncol.* 2015, *33*, (Suppl; Abstr 10564).
15. de Weger, V.; Lolkema, M. P.; Dickson, M.; Le Cesne, A.; Wagner, A.; Merqui-Roelvink, M.; Varga, A.; Tap, W.; Schwartz, G.; Demetri, G.; Zheng, W.; Tuffal, G.; Mace, S.; Miao, H.; Schellens, J. H. M.; de Jonge, M. 378 A first-in-human (FIH) safety and pharmacological study of SAR405838, a novel HDM2 antagonist, in patients with solid malignancies. *Eur. J. Cancer* **2014**, *50*, 121-122.

16. Neochoritis, C.; Estrada-Ortiz, N.; Khoury, K.; Dömling, A. Chapter Twelve - p53–MDM2 and MDMX Antagonists. In *Annu. Rep. Med. Chem.*, Manoj, C. D., Ed.; Academic Press: Burlington 2014; 49, pp 167-187.
17. Popowicz, G. M.; Dömling, A.; Holak, T. A. The structure-based design of Mdm2/Mdmx–p53 inhibitors gets serious. *Angew. Chem., Int. Ed.* **2011**, *50*, 2680-2688.
18. Zhao, Y.; Aguilar, A.; Bernard, D.; Wang, S. Small-molecule inhibitors of the MDM2–p53 protein–protein interaction (MDM2 inhibitors) in clinical trials for cancer treatment. *J. Med. Chem.* **2015**, *58*, 1038-1052.
19. Zak, K.; Pecak, A.; Rys, B.; Wladyka, B.; Dömling, A.; Weber, L.; Holak, T. A.; Dubin, G. Mdm2 and MdmX inhibitors for the treatment of cancer: a patent review (2011 – present). *Expert Opin. Ther. Pat.* **2013**, *23*, 425-448.
20. Khoury, K.; Popowicz, G. M.; Holak, T. A.; Domling, A. The p53-MDM2/MDMX axis - A chemotype perspective. *MedChemComm* **2011**, *2*, 246-260.
21. Gollner, A. The frequent application of multicomponent and cycloaddition reactions for the Synthesis of potent MDM2-p53 inhibitors. *Synlett* **2015**, *26*, 426-431.
22. Sperandio, O.; Reynès, C. H.; Camproux, A.-C.; Villoutreix, B. O. Rationalizing the chemical space of protein–protein interaction inhibitors. *Drug Discovery Today* **2010**, *15*, 220-229.
23. Villoutreix, B. O.; Labbé, C.; Lagorce, D.; Laconde, G.; Sperandio, O. A Leap into the Chemical Space of Protein–Protein Interaction Inhibitors. In *Protein-Protein Interactions in Drug Discovery*, Wiley-VCH Verlag GmbH & Co. KGaA: Weinheim 2013; pp 63-83.
24. Walters, W. P.; Green, J.; Weiss, J. R.; Murcko, M. A. What do medicinal chemists actually make? A 50-year retrospective. *J. Med. Chem.* **2011**, *54*, 6405-6416.
25. Czarna, A.; Beck, B.; Srivastava, S.; Popowicz, G. M.; Wolf, S.; Huang, Y.; Bista, M.; Holak, T. A.; Dömling, A. Robust generation of lead compounds for protein–protein

interactions by computational and MCR chemistry: p53/Hdm2 antagonists. *Angew. Chem., Int. Ed.* **2010**, *49*, 5352-5356.

26. Parks, D. J.; LaFrance, L. V.; Calvo, R. R.; Milkiewicz, K. L.; Gupta, V.; Lattanze, J.; Ramachandren, K.; Carver, T. E.; Petrella, E. C.; Cummings, M. D.; Maguire, D.; Grasberger, B. L.; Lu, T. 1,4-Benzodiazepine-2,5-diones as small molecule antagonists of the HDM2–p53 interaction: discovery and SAR. *Bioorg. Med. Chem. Lett.* **2005**, *15*, 765-770.

27. Rothweiler, U.; Czarna, A.; Krajewski, M.; Ciombor, J.; Kalinski, C.; Khazak, V.; Ross, G.; Skobeleva, N.; Weber, L.; Holak, T. A. Isoquinolin-1-one Inhibitors of the MDM2–p53 Interaction. *ChemMedChem* **2008**, *3*, 1118-1128.

28. Wang, W.; Cao, H.; Wolf, S.; Camacho-Horvitz, M. S.; Holak, T. A.; Dömling, A. Benzimidazole-2-one: A novel anchoring principle for antagonizing p53-Mdm2. *Bioorg. Med. Chem.* **2013**, *21*, 3982-3995.

29. Burdack, C.; Kalinski, C.; Ross, G.; Weber, L.; Khazak, V. Patent WO2010028862A1, 2010.

30. Furet, P.; Kallen, J.; Lorber, J.; Masuya, K. Patent WO2012176123A1, 2012.

31. Ding, K.; Lu, Y.; Nikolovska-Coleska, Z.; Qiu, S.; Ding, Y.; Gao, W.; Stuckey, J.; Krajewski, K.; Roller, P. P.; Tomita, Y.; Parrish, D. A.; Deschamps, J. R.; Wang, S. Structure-based design of potent non-peptide MDM2 inhibitors. *J. Am. Chem. Soc.* **2005**, *127*, 10130-10131.

32. Marugan, J. J.; Leonard, K.; Raboisson, P.; Gushue, J. M.; Calvo, R.; Koblish, H. K.; Lattanze, J.; Zhao, S.; Cummings, M. D.; Player, M. R.; Schubert, C.; Maroney, A. C.; Lu, T. Enantiomerically pure 1,4-benzodiazepine-2,5-diones as Hdm2 antagonists. *Bioorg. Med. Chem. Lett.* **2006**, *16*, 3115-3120.

33. Ivanenkov, Y. A.; Vasilevski, S. V.; Beloglazkina, E. K.; Kukushkin, M. E.; Machulkin, A. E.; Veselov, M. S.; Chufarova, N. V.; Chernyaginab, E. S.; Vanzcool, A. S.; Zyk, N. V.; Skvortsov, D. A.; Khutornenko, A. A.; Rusanov, A. L.; Tonevitsky, A. G.;

- Dontsova, O. A.; Majouga, A. G. Design, synthesis and biological evaluation of novel potent MDM2/p53 small-molecule inhibitors. *Bioorg. Med. Chem. Lett.* **2015**, *25*, 404-409.
34. Kumar, A.; Gupta, G.; Bishnoi, A. K.; Saxena, R.; Saini, K. S.; Konwar, R.; Kumar, S.; Dwivedi, A. Design and synthesis of new bioisosteres of spirooxindoles (MI-63/219) as anti-breast cancer agents. *Biorg. Med. Chem.* **2015**, *23*, 839-848.
35. Yu, B.; Sun, X.-N.; Shi, X.-J.; Qi, P.-P.; Zheng, Y.-C.; Yu, D.-Q.; Liu, H.-M. Efficient synthesis of novel antiproliferative steroidal spirooxindoles via the [3+2] cycloaddition reactions of azomethine ylides. *Steroids* **2015**, *102*, 92-100.
36. Zhou, R.; Wu, Q.; Guo, M.; Huang, W.; He, X.; Yang, L.; Peng, F.; He, G.; Han, B. Organocatalytic cascade reaction for the asymmetric synthesis of novel chroman-fused spirooxindoles that potently inhibit cancer cell proliferation. *Chem. Commun.* **2015**, *51*, 13113-13116.
37. Huang, Y.; Wolf, S.; Bista, M.; Meireles, L.; Camacho, C.; Holak, T. A.; Dömling, A. 1,4-Thienodiazepine-2,5-diones via MCR (I): Synthesis, virtual space and p53-Mdm2 activity. *Chem. Biol. Drug Des.* **2010**, *76*, 116-129.
38. Huang, Y.; Wolf, S.; Beck, B.; Köhler, L.-M.; Khoury, K.; Popowicz, G. M.; Goda, S. K.; Subklewe, M.; Twarda, A.; Holak, T. A.; Dömling, A. Discovery of highly potent p53-MDM2 antagonists and structural basis for anti-acute myeloid leukemia activities. *ACS Chem. Biol.* **2014**, *9*, 802-811.
39. Srivastava, S.; Beck, B.; Wang, W.; Czarna, A.; Holak, T. A.; Dömling, A. Rapid and efficient hydrophilicity tuning of p53/mdm2 antagonists. *J. Comb. Chem.* **2009**, *11*, 631-639.
40. Pettersson, M.; Quant, M.; Min, J.; Iconaru, L.; Kriwacki, R. W.; Waddell, M. B.; Guy, R. K.; Luthman, K.; Grøtli, M. Design, synthesis and evaluation of 2,5-diketopiperazines as inhibitors of the MDM2-p53 interaction. *PLoS ONE* **2015**, *10*, e0137867.

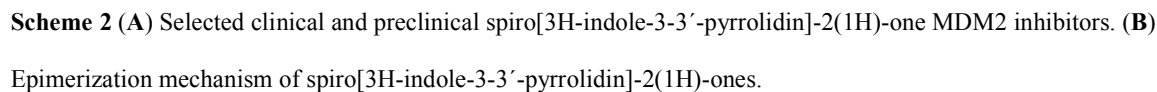
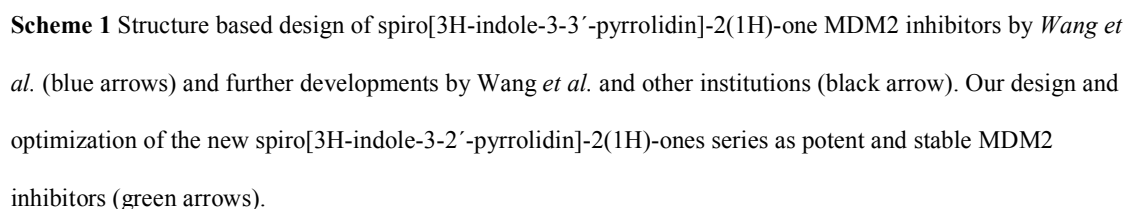
41. Boltjes, A.; Huang, Y.; van de Velde, R.; Rijke, L.; Wolf, S.; Gaugler, J.; Lesniak, K.; Guzik, K.; Holak, T. A.; Dömling, A. Fragment-based library generation for the discovery of a peptidomimetic p53-Mdm4 inhibitor. *ACS Comb. Sci.* **2014**, *16*, 393-396.
42. Zhao, Y.; Liu, L.; Sun, W.; Lu, J.; McEachern, D.; Li, X.; Yu, S.; Bernard, D.; Ochsenbein, P.; Ferey, V.; Carry, J.-C.; Deschamps, J. R.; Sun, D.; Wang, S. Diastereomeric spirooxindoles as highly potent and efficacious MDM2 inhibitors. *J. Am. Chem. Soc.* **2013**, *135*, 7223-7234.
43. Rodrigues, T.; Reker, D.; Schneider, P.; Schneider, G. Counting on natural products for drug design. *Nat. Chem.* **2016**, *8*, 531-541.
44. Antonchick, A. P.; Gerding-Reimers, C.; Catarinella, M.; Schürmann, M.; Preut, H.; Ziegler, S.; Rauh, D.; Waldmann, H. Highly enantioselective synthesis and cellular evaluation of spirooxindoles inspired by natural products. *Nat. Chem.* **2010**, *2*, 735-740.
45. Yu, B.; Yu, D.-Q.; Liu, H.-M. Spirooxindoles: Promising scaffolds for anticancer agents. *Eur. J. Med. Chem.* **2015**, *97*, 673-698.
46. Ding, K.; Lu, Y.; Nikolovska-Coleska, Z.; Wang, G.; Qiu, S.; Shangary, S.; Gao, W.; Qin, D.; Stuckey, J.; Krajewski, K.; Roller, P. P.; Wang, S. Structure-based design of spirooxindoles as potent, specific small-molecule inhibitors of the MDM2-p53 interaction. *J. Med. Chem.* **2006**, *49*, 3432-3435.
47. Wang, S.; Sun, W.; Zhao, Y.; McEachern, D.; Meaux, I.; Barrière, C.; Stuckey, J. A.; Meagher, J. L.; Bai, L.; Liu, L.; Hoffman-Luca, C. G.; Lu, J.; Shangary, S.; Yu, S.; Bernard, D.; Aguilar, A.; Dos-Santos, O.; Besret, L.; Guerif, S.; Pannier, P.; Gorge-Bernat, D.; Debussche, L. SAR405838: An optimized inhibitor of MDM2-p53 interaction that induces complete and durable tumor regression. *Cancer Res.* **2014**, *74*, 5855-5865.
48. Zhang, Z.; Chu, X.-J.; Liu, J.-J.; Ding, Q.; Zhang, J.; Bartkovitz, D.; Jiang, N.; Karnachi, P.; So, S.-S.; Tovar, C.; Filipovic, Z. M.; Higgins, B.; Glenn, K.; Packman, K.;

- Vassilev, L.; Graves, B. Discovery of potent and orally active p53-MDM2 inhibitors RO5353 and RO2468 for potential clinical development. *ACS Med. Chem. Lett.* **2014**, *5*, 124-127.
49. Zhang, Z.; Ding, Q.; Liu, J.-J.; Zhang, J.; Jiang, N.; Chu, X.-J.; Bartkovitz, D.; Luk, K.-C.; Janson, C.; Tovar, C.; Filipovic, Z. M.; Higgins, B.; Glenn, K.; Packman, K.; Vassilev, L. T.; Graves, B. Discovery of potent and selective spiroindolinone MDM2 inhibitor, RO8994, for cancer therapy. *Bior. Med. Chem.* **2014**, *22*, 4001-4009.
50. Nakamaru, K.; Seki, T.; Tazaki, K.; Tse, A. Abstract B5: Preclinical characterization of a novel orally-available MDM2 inhibitor DS-3032b: Anti-tumor profile and predictive biomarkers for sensitivity. *Mol. Cancer Ther.* **2015**, *14*, B5.
51. Huang, W.; Cai, L.; Chen, C.; Xie, X.; Zhao, Q.; Zhao, X.; Zhou, H.-y.; Han, B.; Peng, C. Computational analysis of spiro-oxindole inhibitors of the MDM2-p53 interaction: insights and selection of novel inhibitors. *J. Biomol. Struct. Dyn.* **2016**, *34*, 341-351.
52. Gomez-Monterrey, I.; Bertamino, A.; Porta, A.; Carotenuto, A.; Musella, S.; Aquino, C.; Granata, I.; Sala, M.; Brancaccio, D.; Picone, D.; Ercole, C.; Stiuso, P.; Campiglia, P.; Grieco, P.; Ianelli, P.; Maresca, B.; Novellino, E. Identification of the spiro(oxindole-3,3'-thiazolidine)-based derivatives as potential p53 activity modulators. *J. Med. Chem.* **2010**, *53*, 8319-8329.
53. Bertamino, A.; Soprano, M.; Musella, S.; Rusciano, M. R.; Sala, M.; Vernieri, E.; Di Sarno, V.; Limatola, A.; Carotenuto, A.; Cosconati, S.; Grieco, P.; Novellino, E.; Illario, M.; Campiglia, P.; Gomez-Monterrey, I. Synthesis, in vitro, and in cell studies of a new series of [indoline-3,2'-thiazolidine]-based p53 modulators. *J. Med. Chem.* **2013**, *56*, 5407-5421.
54. Saxena, R.; Gupta, G.; Manohar, M.; Debnath, U.; Popli, P.; Prabhakar, Y. S.; Konwar, R.; Kumar, S.; Kumar, A.; Dwivedi, A. Spiro-oxindole derivative 5-chloro-4',5'-diphenyl-3'-(4-(2-(piperidin-1-yl) ethoxy) benzoyl) spiro[indoline-3,2'-pyrrolidin]-2-one triggers apoptosis in breast cancer cells via restoration of p53 function. *Int. J. Biochem. Cell Biol.* **2016**, *70*, 105-117.

55. Ribeiro, C. J. A.; Amaral, J. D.; Rodrigues, C. M. P.; Moreira, R.; Santos, M. M. M. Synthesis and evaluation of spiroisoxazoline oxindoles as anticancer agents. *Biorg. Med. Chem.* **2014**, *22*, 577-584.
56. Popowicz, G. M.; Czarna, A.; Wolf, S.; Wang, K.; Wang, W.; Dömling, A.; Holak, T. A. Structures of low molecular weight inhibitors bound to MDMX and MDM2 reveal new approaches for p53-MDMX/MDM2 antagonist drug discovery. *Cell Cycle* **2010**, *9*, 1104-1111.
57. Aguilar, A.; Sun, W.; Liu, L.; Lu, J.; McEachern, D.; Bernard, D.; Deschamps, J. R.; Wang, S. Design of chemically stable, potent, and efficacious MDM2 inhibitors that exploit the retro-Mannich ring-opening-cyclization reaction mechanism in spiro-oxindoles. *J. Med. Chem.* **2014**, *57*, 10486-10498.
58. Gollner, A.; Kofink, C.; Ramharter, J.; Weinstabl, H.; Wunberg, T. Patent WO 2015155332, 2015.
59. Gounder, M. M.; Bauer, T. M.; Schwartz, G. K.; Masters, T.; Carvajal, R. D.; Song, S.; Kumar, P.; Gajee, R.; Zernovak, O.; Rosen, M. M.; Kochan, J. P.; Chen, S.; Hyman, D. M.; Gokmen, S.; Meric-Bernstam, F.; LoRusso, P.; Somaiah, N.; Weise, A. M.; Hong, D. S. A phase 1 study of the MDM2 inhibitor DS-3032b in patients (pts) with advanced solid tumors and lymphomas. *J. Clin. Oncol.* 2016, *34*, (Suppl; Abstr 2581).
60. Ray-Coquard, I.; Blay, J.-Y.; Italiano, A.; Le Cesne, A.; Penel, N.; Zhi, J.; Heil, F.; Rueger, R.; Graves, B.; Ding, M.; Geho, D.; Middleton, S. A.; Vassilev, L. T.; Nichols, G. L.; Bui, B. N. Effect of the MDM2 antagonist RG7112 on the P53 pathway in patients with MDM2-amplified, well-differentiated or dedifferentiated liposarcoma: an exploratory proof-of-mechanism study. *Lancet Oncol.* **2012**, *13*, 1133-1140.
61. Information from www.clinicaltrials.gov. Identifier: NCT02143635.

62. Chen, G.; Yang, J.; Gao, S.; Zhang, Y.; Hao, X. Theoretical study of regioselectivity in the synthesis of spiro [pyrrolidine-2,3'-oxindole] compounds by [3+2] cycloaddition. *Res. Chem. Intermed.* **2014**, *41*, 4987-4996.
63. Alimohammadi, K.; Sarrafi, Y.; Tajbakhsh, M.; Yeganegi, S.; Hamzehloueian, M. An experimental and theoretical investigation of the regio- and stereoselectivity of the polar [3+2] cycloaddition of azomethine ylides to nitrostyrenes. *Tetrahedron* **2011**, *67*, 1589-1597.
64. Rajesh, S. M.; Perumal, S.; Menendez, J. C.; Yogeewari, P.; Sriram, D. Antimycobacterial activity of spirooxindolo-pyrrolidine, pyrrolizine and pyrrolothiazole hybrids obtained by a three-component regio- and stereoselective 1,3-dipolar cycloaddition. *MedChemComm* **2011**, *2*, 626-630.
65. Poornachandran, M.; Raghunathan, R. Synthesis of spirooxindolo/spiroindano nitro pyrrolizidines through regioselective azomethine ylide cycloaddition reaction. *Synth. Commun.* **2007**, *37*, 2507-2517.
66. Chen, G.; Yang, J.; Gao, S.; He, H.; Li, S.; Di, Y.; Chang, Y.; Lu, Y.; Hao, X. Spiro[pyrrolidine-2,3'-oxindole] derivatives synthesized by novel regioselective 1,3-dipolar cycloadditions. *Mol. Diversity* **2011**, *16*, 151-156.
67. Poornachandran, M.; Muruganatham, R.; Raghunathan, R. Regioselective synthesis of novel spirooxindolo and spiroindano nitro pyrrolidines through 3+2 cycloaddition reaction. *Synth. Commun.* **2006**, *36*, 141-150.
68. Krasovskiy, A.; Knochel, P. A LiCl-mediated Br/Mg exchange reaction for the preparation of functionalized aryl- and heteroarylmagnesium compounds from organic bromides. *Angew. Chem., Int. Ed.* **2004**, *43*, 3333-3336.
69. Krasovskiy, A.; Straub, B. F.; Knochel, P. Highly efficient reagents for Br/Mg exchange. *Angew. Chem., Int. Ed.* **2006**, *45*, 159-162.

Prior work by Wang *et al.*: Spiro[3H-indole-3,3'-pyrrolidin]-2(1H)-ones



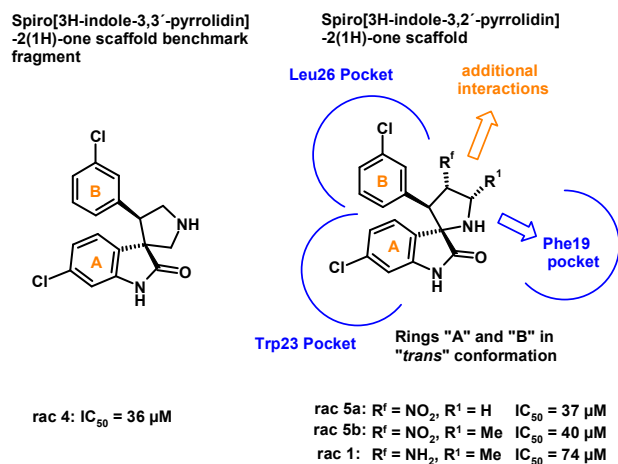
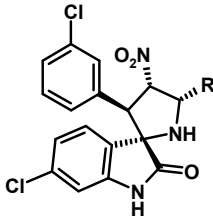
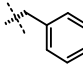
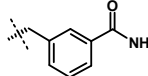
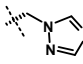
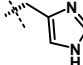
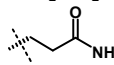


Figure 1. Benchmark fragment **rac 4** and first spiro[3H-indole-3,2'-pyrrolidin]-2(1H)-ones.

Table 1. R^1 substitution SAR for spiro[3H-indole-3,2'-pyrrolidin]-2(1H)-ones.



| Compound | R^1 | IC_{50} (MDM2-p53) [μM] ^a |
|----------|---|--|
| rac 5a | -H | 36.5 |
| rac 5b | -CH ₃ | 40.1 |
| rac 5c | -CH ₂ SCH ₃ | 24.6 |
| rac 5d |  | 15.6 |
| rac 5e |  | 18.3 |
| rac 5f |  | 5.5 |
| rac 5g |  | 15.2 |
| rac 5h | -CH ₂ OH | 30.7 |
| rac 5i | -CH ₂ CH ₂ OH | 16.0 |
| rac 5j | -CH ₂ CO ₂ H | 18.6 |
| rac 5k |  | 13.5 |

^aValues are expressed as mean of at least two measurements.

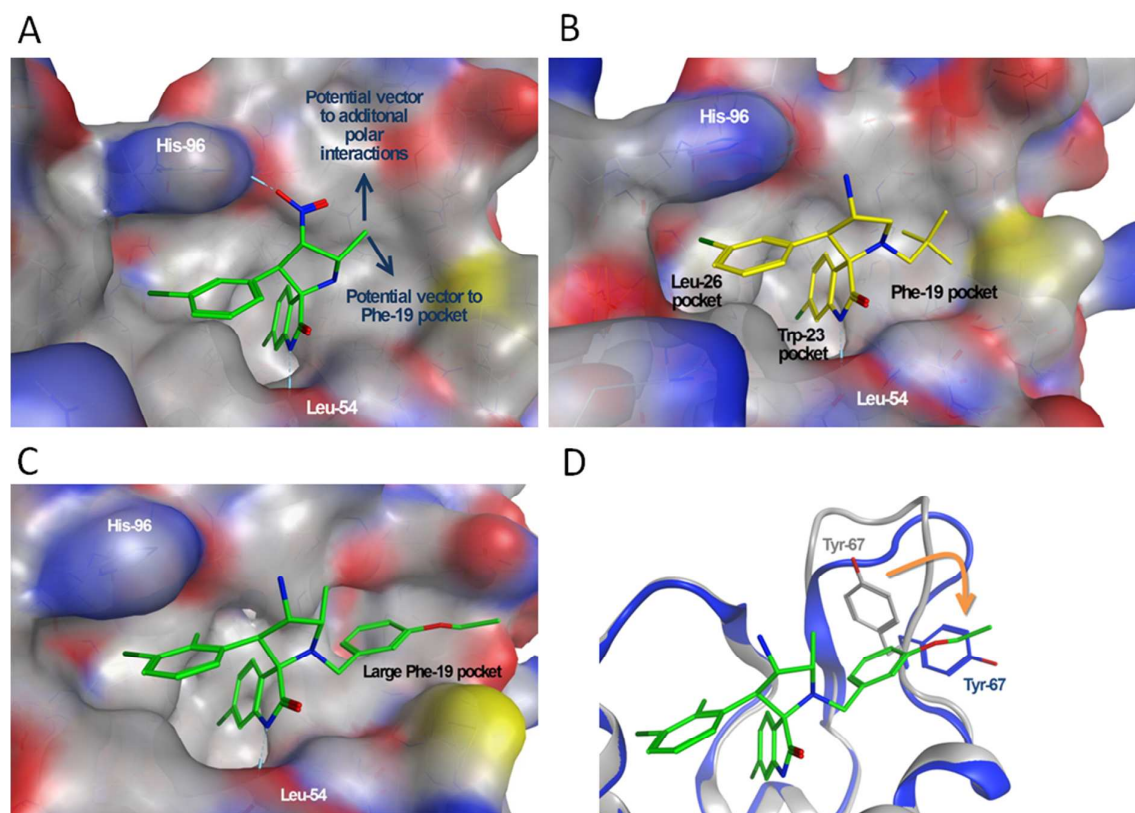


Figure 2. (A) Docking of **5b** (green) in 3LBL. Potential vectors for additional interactions are indicated with blue arrows. (B and C) X-ray co-crystal structures of **6b** (B, yellow) and **6g** (C, green) in MDM2. (B) The Leu26, Trp23 and Phe19 pockets are indicated as well as the key hydrogen bond interaction of **6b** with Leu54. The 2-chlorophenyl fills the Leu26 pocket, the oxindole is buried in the Trp23 pocket while the t-butyl-group occupies the Phe19 pocket.(C) The ethoxy-benzyl substituent of **6g** (green) causes a change in the protein conformation and leads to an enlarged Phe19 pocket. (D) Tyr67 flips from the Tyr-in in a Tyr-out conformation as observed in the X-ray co-crystal structure of **6g** (green, MDM2 protein indicated as blue ribbon) compared the structure of **6b** (ligand not shown, MDM2 protein indicated as gray ribbon). Compound **6b**: PDB code 5LAV; compound **6g**: PDB code 5LAY.

Table 2. R¹, R² and R³ substitution SAR for spiro[3H-indole-3,2'-pyrrolidin]-2(1H)-ones

| Compound | R ¹ | R ² | R ³ | IC ₅₀ (MDM2-p53) [nM] ^a |
|----------|----------------|----------------|----------------|--|

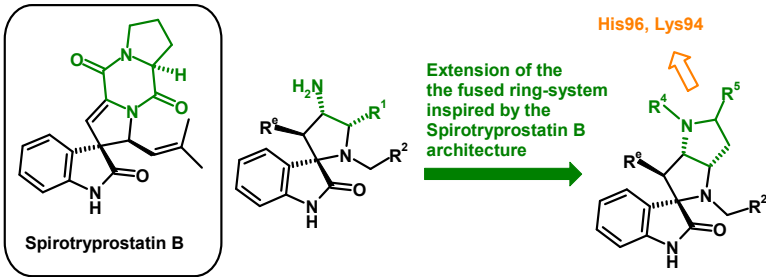
| | | | | |
|--------|------------------|--|----|------|
| 6a | -H | | -H | 944 |
| 6b | -H | | -H | 819 |
| rac 6c | -CH ₃ | | -H | 1075 |
| 6d | -CH ₃ | | -H | 563 |
| 6e | -CH ₃ | | -F | 157 |
| rac 6f | | | -H | 2064 |
| rac 6g | -CH ₃ | | -F | 57 |
| 6g | -CH ₃ | | -F | 34 |

^aValues are expressed as mean of at least two measurements.

Table 3. R⁴ substitution SAR for spiro[3H-indole-3,2'-pyrrolidin]-2(1H)-ones

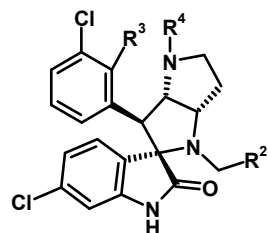
| Compound | R ⁴ | IC ₅₀ (MDM2-p53) [nM] ^a |
|----------|------------------------------------|--|
| 6e | -H | 157 |
| 8 | -COCH ₃ | 229 |
| 9 | -CH ₂ CO ₂ H | 62 |
| 2 | | 107 |

^aValues are expressed as mean of at least two measurements.



Scheme 3. Fusion of the spiro[3H-indole-3,2'-pyrrolidin]-2(1H)-ones ring-system to generate better vectors to address polar interactions with His96 and Lys94 inspired by Spirotryprostatin B

Table 4. R⁴ and R² substitution SAR for octahydro-1'H-spiro[indole-3,2'-pyrrolo[3,2-b]pyrrole]-2-ones



| Compound | R ² | R ⁴ | R ³ | IC ₅₀ (MDM2-p53) [nM] ^a |
|---------------|----------------|------------------------------------|----------------|---|
| 10 | | -H | -F | 137 |
| rac 11 | | -COCH ₃ | -F | 212 |
| rac 12 | | -CH ₂ CO ₂ H | -F | 39 |
| 13 | | -CH ₂ CO ₂ H | -F | 2 |
| rac 14 | | -CH ₂ CO ₂ H | -H | 80 |

^aValues are expressed as mean of at least two measurements.

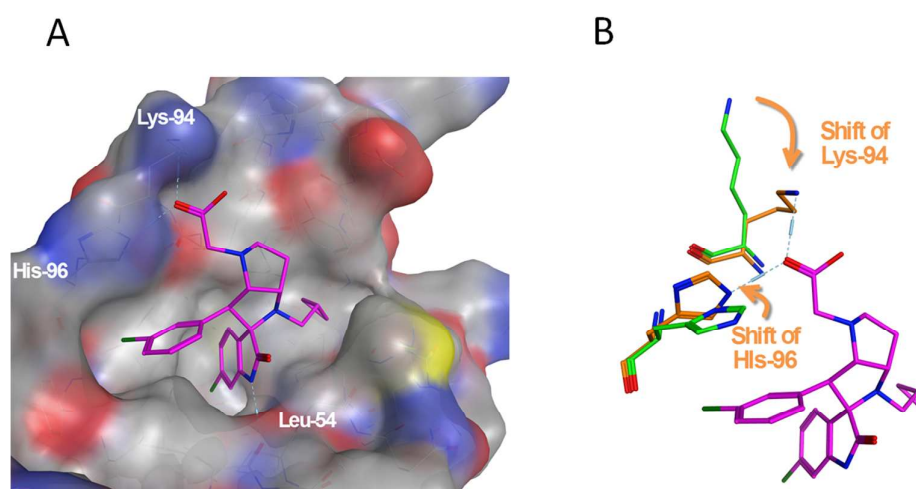
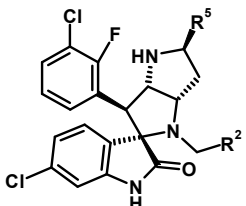

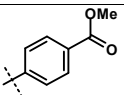

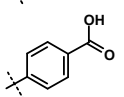

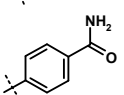
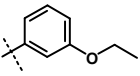
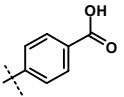


Figure 3. (A) X-ray co-crystal structure of **14** (magenta) in MDM2. (The racemic compound **rac 14** was used for crystallization, only the eutomer **14** was found in the co-crystal structures.) (B) The amino acids His96 and Lys94 are shown as orange sticks, the hydrogen bonds with the carboxylic acid of **14** (magenta) with His96 and

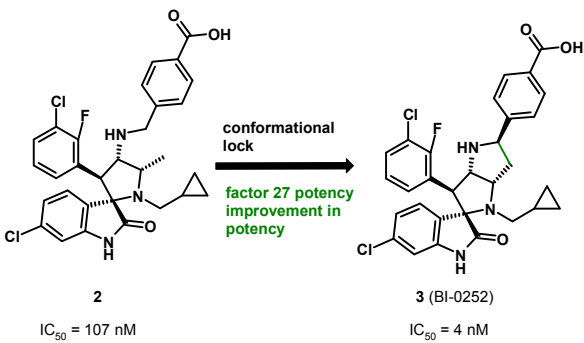
Lys94 are indicated. A strong shift of the amino acid side chains of His96 and Lys94 is observed when compared to the structure of **6b** (ligand not shown, selected MDM2 amino acids in green). Compound **14**: PDB code 5LAW.

Table 5. R² and R⁵ substitution SAR for octahydro-1'H-spiro[indole-3,2'-pyrrolo[3,2-b]pyrrole]-2-ones



| Compound | R ² | R ⁵ | IC ₅₀ (MDM2-p53) [nM] ^a |
|----------|---|---|---|
| 15 |  |  | 81 |
| 3 |  |  | 4 |
| 16 |  |  | 16 |
| 17 |  |  | 2 |

^aValues are expressed as mean of at least two measurements.



Scheme 4. Potency gain by the introduction of an octahydro-pyrrolo[3,2-b]pyrrole ring system.

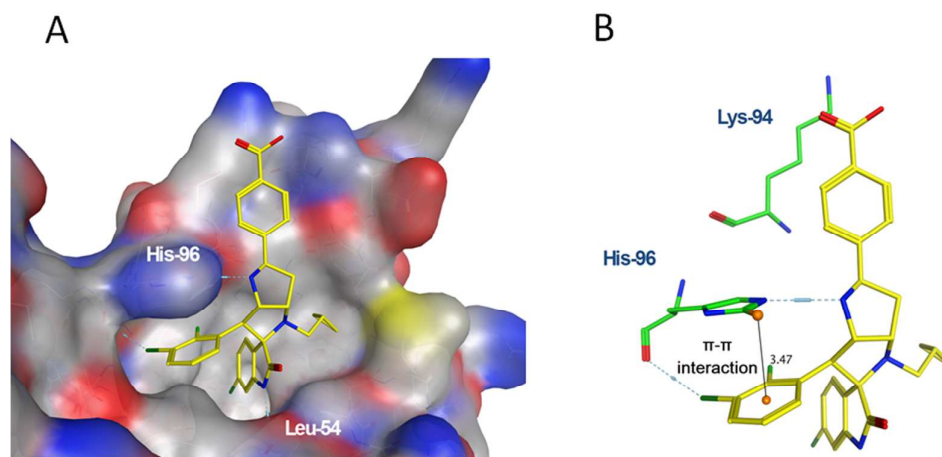


Figure 4. (A) X-ray co-crystal structure of **3** (yellow) in MDM2. (The racemic compound **rac 3** was used for crystallization, only the eutomer **3** was found in the co-crystal structures.) (B) The key interactions of **3** (yellow) with His96 are highlighted. The π - π interaction is indicated by the orange spheres and the black line (distance 3.47 Å). Compound **3**: PDB code 5LAZ.

Table 6. Cellular potency of selected compounds on SJSA-1 (p53 WT) and SK-OV-3 (p53 mut) cell lines.

| Compound | IC ₅₀ (MDM2-p53)[nM] ^a | IC ₅₀ [SJSA-1 CTG (p53 WT)] [nM] ^a | IC ₅₀ [SK-OV-3 Alamar (p53 mut)] [nM] ^a |
|-----------|--|--|---|
| 6e | 157 | 2980 | >25000 |
| 9 | 62 | 2879 | >25000 |
| 10 | 137 | 2609 | >25000 |
| 13 | 2 | 287 | >25000 |
| 3 | 4 | 471 | >25000 |
| 16 | 16 | 1447 | >25000 |
| 17 | 2 | 67 | >25000 |

^aValues are expressed as mean of at least two measurements.

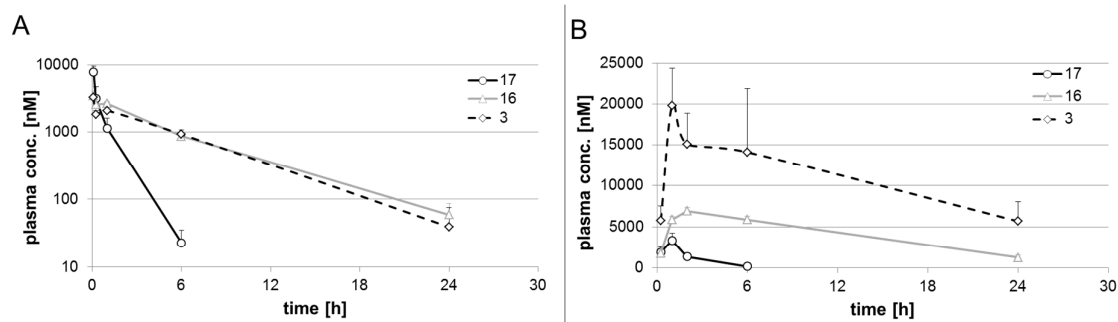


Figure 5. Plasma PK profiles after single administration of compounds **3** (black diamonds), **16** (grey triangles) and **17** (black circles) in non-tumor-bearing female NMRI nude mice. Plasma concentrations were determined by

LC/MS/MS. Error bars indicate standard deviations in plasma concentrations from 3 animals per dose group per compound **(A)** iv PK profiles after a single 5 mg/kg iv bolus dose, formulated in 25% HP- β -CD, 10 ml/kg application volume **(B)** po PK profiles after a single 50 mg/kg po dose formulated in 0.5% Natrosol (pH 7-8, NaOH titrated), 10 ml/kg application volume

Table 7. Single administration iv and po mean PK parameters determined by non-compartmental analysis in female NMRI nude mice. AUC values were calculated using linear trapezoidal interpolation

| Compound | po dose [mg/kg] | po AUC _{0-24h} [μ M*h] | po conc _{max} [μ M] | iv dose [mg/kg] | CL [mL/min/kg] | Vss [L/kg] | F% [%] |
|-----------|--------------------|--|---|-----------------------|-------------------|---------------|-----------|
| 3 | 50 | 264 | 21.3 | 5 | 7.1 | 2.1 | - |
| 16 | 50 | 100 | 6.9 | 5 | 7.4 | 2.0 | 58 |
| 17 | 50 | 8 | 3.4 | 5 | 23.2 | 1.0 | 13 |

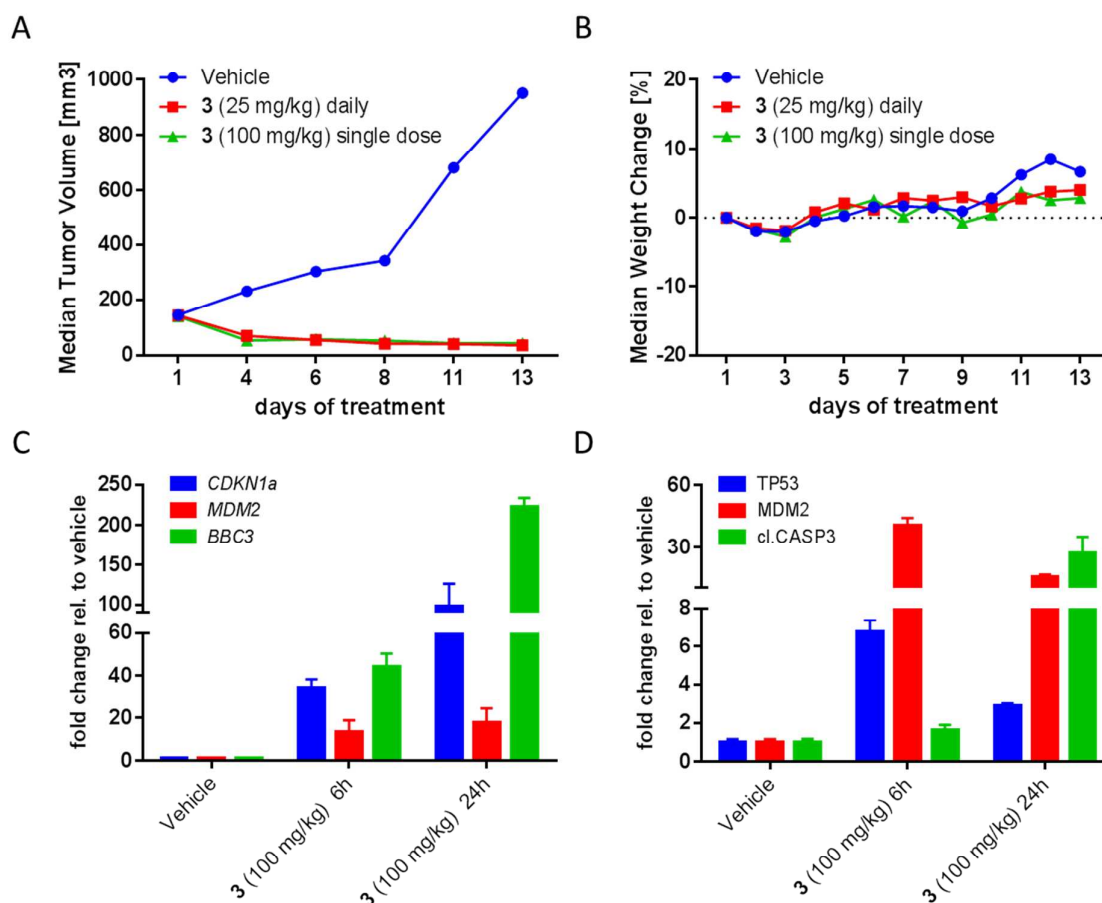


Figure 6. Efficacy of compound 3 in a sc SJSA-1 osteosarcoma xenograft model. (A, B) NMRI nude mice bearing established subcutaneous SJSA-1 tumors were treated orally with either vehicle (blue circles) or with compound 3 at 25 mg/kg daily (red squares) or with a single dose of compound 3 at 100 mg/kg (green triangles). Median tumor volumes of 8 animals per treatment group (A) and median body weight changes in % of initial weight (B) are shown. (C, D, E) NMRI nude mice bearing established subcutaneous SJSA-1 tumors were treated orally with either vehicle or with a single dose of compound 3 at 100 mg/kg, and tumors were harvested either 6h or 24h after compound administration for (C) mRNA or (D) protein biomarker analysis.

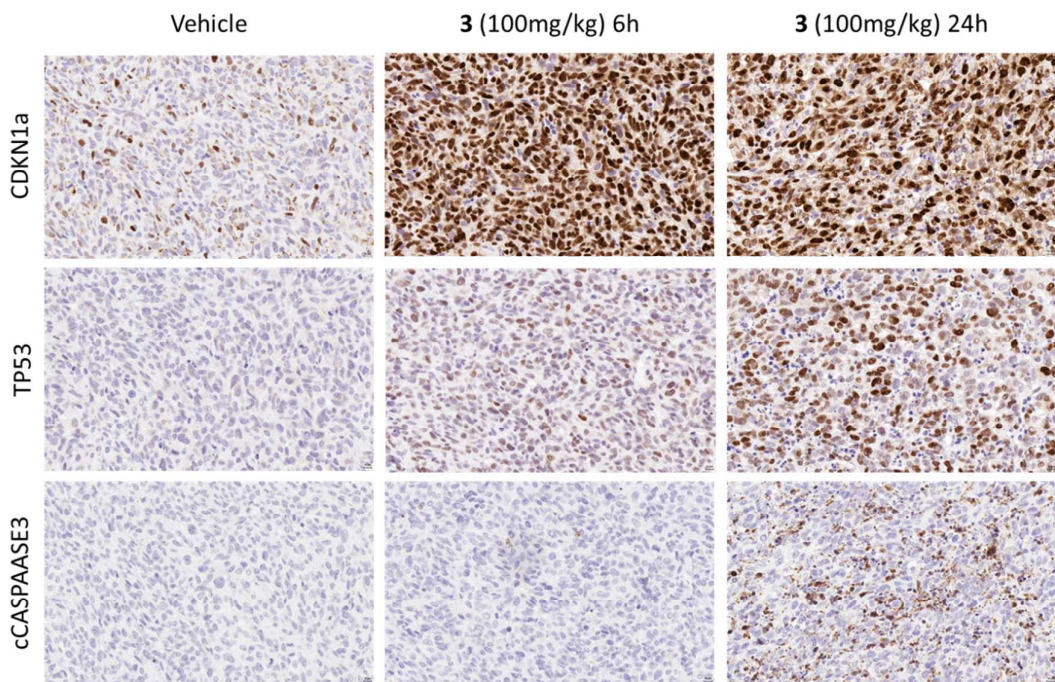
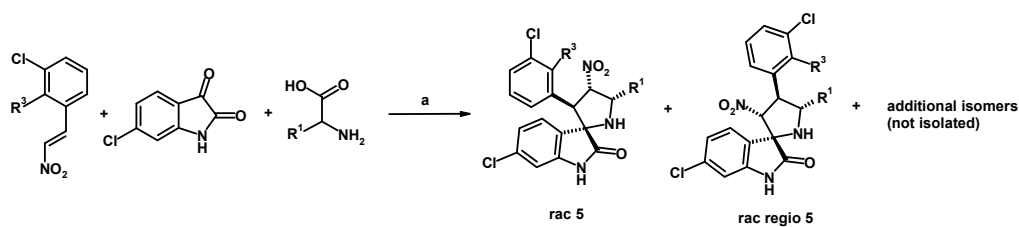


Figure 7. Immunohistochemical (IHC) analysis of SJSA-1 tumor samples. SJSA-1 tumor bearing NMRI nude mice were treated with a single oral dose of compound **3** (100 mg/kg). Tumors were harvested 6 and 24h post dose and IHC staining was performed for CDKN1a (a TP53 target gene) (**top**), TP53 (**middle**) and cleaved CASPASE3, a biomarker of apoptosis induction (**bottom**).

Table 8. Dipolar cycloaddition of nitrostyrenes, isatins and amino acids.^a

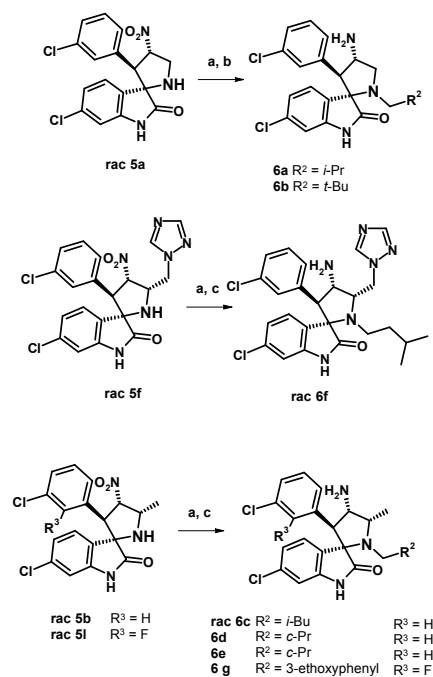


| Entry | R ¹ | R ³ | (%) | (% regio) |
|---------------|-----------------------------------|----------------|-----|-----------|
| rac 5a | -H | -H | 2 | 48 |
| rac 5b | -CH ₃ | -H | 63 | 12 |
| rac 5c | -CH ₂ SCH ₃ | -H | 33 | 31 |
| rac 5d | -Bn | -H | 53 | 19 |
| rac 5e | | -H | 11 | 5 |
| rac 5f | | -H | 59 | 15 |
| rac 5g | | -H | 10 | 6 |
| rac 5h | -CH ₂ OH | -H | 32 | 34 |

| | | | | |
|---------------|--|----|----|-----------------|
| rac 5i | -CH ₂ CH ₂ OH | -H | 48 | 16 |
| rac 5j | -CH ₂ CO ₂ H | -H | 5 | 2 |
| rac 5k | -CH ₂ CH ₂ CONH ₂ | -H | 36 | 7 |
| rac 5l | -CH ₃ | -F | 52 | 12 |
| rac 5m | -CH ₂ CH ₂ OH | -F | 46 | not isolated |

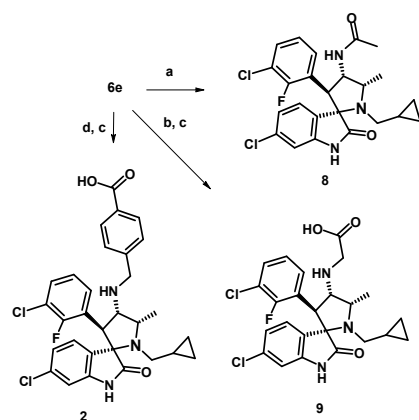
^a Reagents and conditions: (a) MeOH, reflux.

Scheme 5. Synthesis of compounds **6a-g**^a

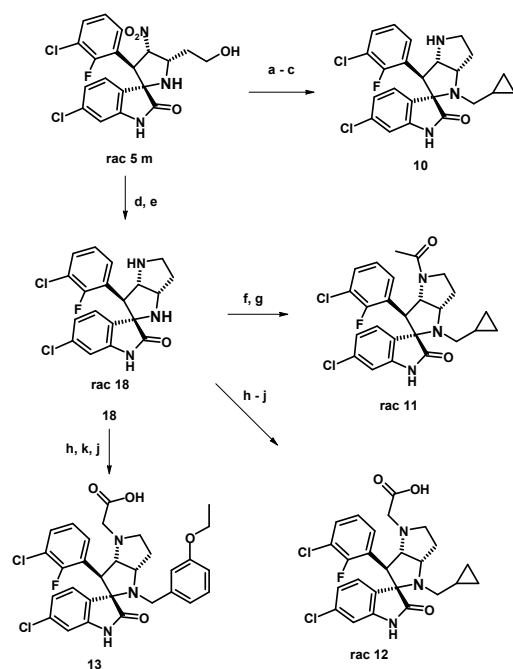


^a Reagents and conditions: (a) $R_2\text{CHO}$, CH₃CN, AcOH, NaBH(OAc)₃, 30–76%; (b) Raney Ni, H₂, MeOH, 21–22%; (c) In, HCl, THF, rt, 54–82%, enantiomer separation by chiral SFC.

Scheme 6^a

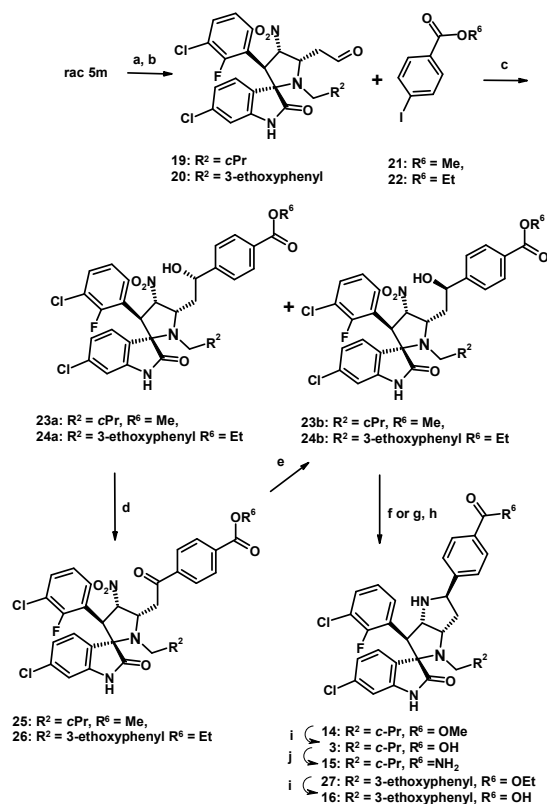


^a (a) AcOH, HATU, DIPEA, DMF, rt, 76%; (b) glyoxylic acid ethyl ester in PhMe, NaBH(OAc)₃, DMF, rt, 30%; (c) NaOH, THF, rt, H₂O, 67–70%; (d) methyl 4-formylbenzoate, NaBH(OAc)₃, DMF, rt, 65%.

Scheme 7^a

^a (a) *c*-PrCHO, DMF, AcOH, NaBH(OAc)₃, rt, 18 h, 92% (b) In, HCl, THF, rt, 18 h, 93%; (c) DEAD, PPh₃, DCM, rt, 1 h, 37%, enantiomer separation by chiral SFC; (d) Raney Ni, H₂, MeOH, 18 h, 56%; (e) DEAD, PPh₃, DCM, rt, 1 h, 46%, enantiomer separation by chiral SFC; (f) AcOH, HATU, DIPEA, DMF, rt, 63%; (g) *c*-PrCHO, CH₃CN, AcOH, NaBH(OAc)₃, rt, 2 h, 18%, (h) glyoxylic acid ethyl ester in PhMe, NaBH(OAc)₃, DMF, rt, 18 h, 25–53%; (i) *c*-PrCHO, CH₃CN, AcOH, NaBH(OAc)₃, rt, 18 h, 27%; (j) NaOH, THF, H₂O, rt, 18 h, 82–97%, (k) 3-ethoxybenzaldehyde, CH₃CN, AcOH, NaBH(OAc)₃, rt, 18 h, 78%.

Scheme 8^a



^a (a) RCHO, DMF, AcOH, NaBH(OAc)₃, rt, 18 h, 66–92%; (b) IBX, CH₃CN, 75 °C, 1 h, 93–94%; (c) 4-I-PhCO₂R⁶, *i*-PrMgCl·LiCl, THF, -40 °C to rt, for $R^2 = c\text{-Pr}$: **23a** 64% and **23b** 18%, for $R^2 = 3\text{-ethoxyphenyl}$: **24a** 55% and **24b** 12%; (d) IBX, CH₃CN, 75 °C, 2 h, 92–98%; (e) NaBH₄, CH₃OH, 0 °C, 6 h, for $R^2 = c\text{-Pr}$: **23a** (36%) and **23b** (47%), for $R^2 = 3\text{-ethoxyphenyl}$: **24a** 17% and **24b** 41%; (f) Raney Ni, H₂, MeOH, 18 h, 75% for **14**; (g) In, HCl, THF, rt, 18 h, 74% for **25**; (h) DEAD, PPh₃, DCM, rt, 1 h, 75–84% (i) NaOH, THF, H₂O, rt, 18 h, 84–90%, (j) HATU, DIPEA, NH₃, DMF, rt, 30 min, 60%.

TABLE OF CONTENT GRAPHIC

